Master's thesis

NTNU
Norwegian University of Science and Technology
Faculty of Information Technology and Electrical Engineering
Department of Electric Power Engineering

Nina Lindholm

Islanded Microgrids: a Predictive Approach to Control Operation

Master's thesis in Energy and Environmental Engineering
Supervisor: Jayaprakash Rajasekharan
June 2020

NTNU
Norwegian University of Science and Technology

TrønderEnergi

Nina Lindholm

Islanded Microgrids: a Predictive Approach to Control Operation

Master's thesis in Energy and Environmental Engineering
Supervisor: Jayaprakash Rajasekharan
June 2020

Norwegian University of Science and Technology
Faculty of Information Technology and Electrical Engineering
Department of Electric Power Engineering

NTNU
Norwegian University of
Science and Technology

Abstract

Building an island mode operated microgrid is a solution to supply remote areas with electricity. In order to contribute to the decarbonization, fossil fuel solutions are not an option. Weather dependent energy sources are common, in order to make these microgrids renewable. To compensate for their intermittent behaviour power predictions are useful.

A case study is conducted on Rye microgrid in Norway. Predictions of the power from photovoltaic panels, a wind turbine and a load are made. The storage units in the microgrid are a battery energy storage system and a hydrogen energy storage system (electrolyser, tank and fuel cell). A diesel generator set is also included for backup.

In this thesis, a new operational strategy for the microgrid is developed. The new design is inspired by Model Predictive Control. Power predictions are made, based on basic machine learning concepts. The prediction models are trained on historical measurements of environmental data and time stamps. In every time step, the predictions are made for a certain control horizon. These predictions are input into an optimisation, that is executed to determine the power of all involved components. The first time step of the optimisation result is applied to the microgrid. In order to do so, a balancing of powers is done, to make up for inaccuracies in the predictions. The process is repeated for every hour of a year.

The results clarify the importance of having a good control system. The objective function's main focus was to limit the power from the diesel generator. In addition, it limited the amount of curtailed power from the generating units. The final priority was to limit the energy lost in conversion related to the battery, electrolyser and fuel cell. The predictive control greatly influences the operation, and having an objective function makes the system strategy easy to alter. Comparing the developed model with the existing model, the energy supplied by the diesel generator was reduced by 48.71%. These results bring the microgrid closer to meeting its goal of limiting the diesel dependence.

As a consequence, changing the operational strategy may have an impact on the microgrid success. It could be considered a valuable design feature in new and established microgrids. The final hope is for this thesis to contribute to renewable energy being available, even in remote locations.

Sammendrag

Bygging av mikronett i øydrift er et alternativ for å levere energi til avsidesliggende områder. For å bidra til det grønne skiftet er alternativer som bruker fossile brennstoff ikke aktuelle. Væravhengige energikilder er vanlige å bruke for å gjøre mikronett fornybare. For å kompensere for deres varierende generering er prediksjoner nyttige.

Et casestudie er utført på Rye Mikronett i Trondheim. Prediksjoner av effekt fra fotovoltaiske paneler, en vindturbin og last er utført. Lagringsenhetene i mikronettet er et batteri og et hydrogensystem (elektrolysør, tank og brenselcelle). En dieselgenerator er installert som reserveløsning.

I denne oppgaven har det blitt utviklet en ny operasjonsstrategi. Det nye designet er inspirert av Model Predictive Control. Effektprediksjoner er laget, basert på enkle maskinlæringskonsepter. Prediksjonsmodellene er trent på historiske målinger av værdata og tidspunkter. I hvert tidssteg blir prediksjonene over en viss tidshorisont laget. Disse prediksjonene blir tatt med i en optimering for å bestemme hver enkelt komponents effekt. Det første tidssteget fra optimeringsresultatet blir utført. Før dette kan gjøres må effektene balanseres på nytt, for å gjøre opp for feil i prediksjonene. Prosessen blir gjentatt for hver time i ett år.

Resultatene tydeliggjør viktigheten av et godt styringssystem. Optimeringens objektivfunksjon sitt hovedfokus var å begrense bruken av dieselgeneratoren. I tillegg ble mengden kuttet energi fra solcellepanelene og vindmøllen begrenset. Den siste prioriteringen var å begrense mengden tapt energi i omgjøringene i batteri, elektrolysør og brenselcelle. Den prediktive metoden har stor innvirkning på hvordan mikronettet opereres. Ved den implementerte objektivfunksjonen er det enkelt å endre strategien. Sammenligning av den nye, prediktive metoden med den eksisterende strategein, viser at energien fra dieselgeneratoren blir redusert med 48.71%. Disse resultatene reduserer mikronettets dieselavhengighet.

Som en konsekvens av dette kan endringene i styringssystemet ha en effekt på mikronettets suksess. Det kan bli et verdifullt tillegg i både nye og eksisterende mikronett. Håpet er at denne oppgaven kan bidra til å gjøre fornybar energi tilgjengelig, særlig i avsidesliggende områder.

Acknowledgement

Upon the completion of this master thesis, several people must be thanked. It was written at the Department of Electric Power Engineering at the Norwegian University of Science and Technology (NTNU). Here, my main supervisor, Jayaprakash Rajasekharan, deserves much praise. Thank you for all the engagement, from the beginning and until the very end. Your knowledge and willingness to help has been vital. To help with the implementation in Python and Pyomo, Kasper Emil Thorvaldsen has been a significant resource.

TrønderEnergi initiated the microgrid project and have been great collaborational partners. Your fast response and willingness to help has been of great use. Especially Anniken Auke Borgen and Bernhard Kvaal.

At last I would like to applaud my friends and family for all the fun and support.

Thank you.

Table of Contents

Abstract i

Sammendrag ii

Acknowledgement iii

1 Introduction 1

1.1 Context . . . 1

1.2 Motivation . . . 1

1.3 Scope of work . . . 2

1.4 Report outline . . . 3

2 Background 4

2.1 Microgrid operation . . . 4

2.2 Model Predictive Control . . . 5

2.3 Power prediction . . . 6

3 Case Study: Rye Microgrid 9

3.1 Overview . . . 9

3.2 Wind turbine . . . 10

3.3 Photovoltaic system . . . 11

3.4 Battery . . . 12

3.5 Hydrogen system . . . 13

3.5.1 Electrolyser . . . 13

3.5.2 Hydrogen tank . . . 14
3.5.3 Fuel cell . . . 14
3.6 Load . . . 15
3.7 Backup system . . . 17

4 Modelling of Microgrid Operational Control **18**
4.1 Base case management . . . 18
4.1.1 Control logic . . . 18
4.1.2 Component simulation . . . 20
4.2 Predictive control . . . 22
4.2.1 Predictions . . . 22
4.2.2 Implementation . . . 23
4.3 Code architecture . . . 29
4.3.1 File hierarchy . . . 29
4.3.2 Pseudocode . . . 31
4.3.3 Code robustness . . . 32
4.4 Data preparation . . . 32

5 Results **35**
5.1 Base case . . . 35
5.1.1 Power balance . . . 35
5.1.2 Component utilisation . . . 36
5.2 Predictive control system . . . 38
5.2.1 Predictions . . . 38
5.2.2 Objective function . . . 41
5.2.3 Component utilisation . . . 42
5.2.4 Run time . . . 44
5.3 Comparison of behaviour . . . 45

6 Discussion and Future Work **49**

6.1 Evaluation of operation 49
6.2 Modelling shortcomings and strengths 50
6.3 General learning outcomes 52
6.4 Future work 52

7 Conclusion **54**

Bibliography **54**

Appendix **61**

List of Figures

1.1 The goals, problems and solutions at hand for the thesis. The thesis combines the two solutions, microgrid and power predictions, into a new operational strategy. 2

2.1 Illustration of the three levels of a hierarchical control structure. Inspired by fig 3 in [1]. . 5

2.2 Common procedure of forecasting generation from renewable, weather dependent sources. Adapted from Fig 1 in [2]. 6

2.3 Simplified illustration of a Regression Tree. Inspired by [3]. 6

3.1 Pictures of the microgrid being set up at Rye, Norway. Taken by Bernhard Kvaal, TrønderEnergi. 9

3.2 Overview of the most important components of the microgrid at Rye, excluding some technical components.[4, 5] 10

3.3 Measured monthly and yearly energy generation from wind turbine at Rye [6]. Note that the turbine was out of operation during the summer of 2017. 11

3.4 Energy generation from the solar system at Rye. Measurements from on site and estimations by SolarEdge [7]. 12

3.5 Battery system configuration. Inspired by [8]. The grey box is the inverter that connects the alternative current (AC) side of the microgrid to the direct current (DC) battery. . . . 13

3.6 Electrolyser efficiency vs. power (% of nominal), inspired by graph in [9]. 14

3.7 Fuel cell efficiency vs. power, inspired by graph in [9]. 15

3.8 Energy consumption of load at farm 30/4-19 - 29/4/20, aggregated to monthly levels. . . 16

3.9 Hourly power demand at farm, 30/4-19 - 29/4/20. 16

4.1 Overview of modelling of the base case control structure. Input powers in the green box, sharing logic in the orange and resulting output in the blue boxes. 19

4.2 Flow chart of control logic for the base case. Elaboration of the previous figure. 19

4.3 General description of the predictive control algorithm. The current time step is denoted t, while H is the contorl horizon. 24

4.4 An overview of the microgrid and all the simulated powers. The direction of the arrow defines the positive direction. 25

4.5 Flow chart of the implemenation of applying the control action. It describes the balancing of the power difference between optimised and real available powers. 29

4.6 File hierarchy of the simulation. These files hold everything necessary for modelling both control systems of the microgrid. The orange box holds the main folders, and the blue boxes the relevant subfolders. 30

4.7 Implementation of the predictive control and the relations between the different nodes. The orange texts are functions, the grey boxes are folders or files and the blue circles are function calls. The current time step in the simulation is t, while the control horizon is denoted H. 31

4.8 Conceptual sketch of the backup solution to ensure code robustness. 32

5.1 Input powers of the system. The generation of PV and wind and the load of the system on an hourly basis. 35

5.2 Base case hourly states of the different components. (a) Battery states. Charging, discharging and idleness. (b) Hydrogen states. Electrolyser, fuel cell and idleness. (c) Generator states. ON and OFF. 36

5.3 Energy level in the battery (SoC) and hydrogen tank (H2 tank) over the entire year for the base case simulation. 37

5.4 The predicted and real power of the PV-panels at Rye. The blue are the real measured values on site, and the orange are predicted by a machine learning algorithm. 39

5.5 The predicted and real power of the wind turbine at Rye. The blue are the real measured values on site, and the orange are predicted by a machine learning algorithm. 40

5.6 The predicted and real power of the load at Rye. The blue are the real measured values on site, and the orange are predicted by a machine learning algorithm. 41

5.7 Predictive hourly states of the different components. (a) Battery states. Charging, discharging and idleness. (b) Hydrogen states. Electrolyser, fuel cell and idleness. (c) Generator states. ON and OFF. 43

5.8 Energy level in the battery (SoC) and hydrogen tank (H2 tank) over the entire year. From the predictive simulation. 44

5.9 Comparison between the two designed control systems (Base case and Predictive). It shows how the battery (SoC) and hydrogen (H2 tank) run empty i the base case, leading to the diesel generator (Gen) being used. In the predictive control this is prevented. . . . 46

5.10 Comparison between the two designed control systems (Base case and Predictive) for two weeks in April. It shows how the battery (SoC) and hydrogen (H2 tank) run empty in both cases. The usage of the diesel generator (Gen) varies significantly between the two. In the base case, the generator is always operated at maximum power. In the predictive, the diesel power usage varies with the load. 47

5.11 Comparison between the two designed control systems (Base case and Predictive) for two weeks in April. It shows how the battery (SoC) and hydrogen (H2 tank) are rather full. The variation in solar power (PV) and wind power (Wind) is also shown. The predictive control seems to have unnecessary large variation in both the battery and the hydrogen level. 48

7.1 Data structures within the code for basecase control. 61

List of Tables

3.1 Specifications of the wind turbine at Rye microgrid[10, 11] 10

3.2 Specifications of the photovoltaic system at Rye microgrid[12]. 11

3.3 Specifications of the battery at Rye microgrid[5, 8] 12

3.4 Specifications of the electrolyser at Rye microgrid[11] 13

3.5 Specifications of the fuel cell at Rye microgrid[9] 15

4.1 Lower and upper bounds of power variables.[13][8][9] 27

4.2 The dates from which the different data is gathered by each component. 33

4.3 Monthly average consumption and factor multiplied with data from March to generate consumption data from the circuit by the pigs barn. 33

5.1 Accuracy of PV prediction model when ran on simulation data (2019 and 2020). Normalized mean average error (nMAE), normalized root mean square error (nRMSE) and coefficient of determination (R^2). 38

5.2 Accuracy of wind prediction model when ran on new data (2019 and 2020). Normalized mean average error (nMAE), normalized root mean square error (nRMSE) and coefficient of determination (R^2). 39

5.3 Accuracy of load prediction model when ran on new data (2019 and 2020). Normalized mean average error (nMAE), normalized root mean square error (nRMSE) and coefficient of determination (R^2). 40

5.4 Different objective function weights (eq. (4.12)) and their impact on central evaluation criteria. Tested for 1500 hours. Diesel coverage (eq. (5.2)), PV curtailment (eq. (5.5)), Wind curtailment (eq. (5.6)), Fuel cell coverage (eq. (5.4)), Battery coverage (eq. (5.3)). . 41

5.5 Comparison between the two systems: base case and predictive control system. Absolute values of the amount of energy the component supplies over the entire year. 45

Abbreviations

AC	=	Alternating Current
DC	=	Direct Current
BESS	=	Battery Energy Storage System
EU	=	European Union
FC	=	Fuel cell
HESS	=	Hydrogen Energy Storage System
LHV	=	Lower Heating Value
MAE	=	Mean Absolute Error
MSE	=	Mean Squared Error
MG	=	Microgrid
ML	=	Machine Learning
MPC	=	Model Predictive Control
nMAE	=	Normalized Mean Absolute Error
NOK	=	Norwegian Kroner
nRMSE	=	Normalized Root Mean Square Error
PEM	=	Proton-Exchange Membrane
PV	=	Photovoltaic solar panels
R^2	=	Coefficient of Determination
SoC	=	State of Charge (battery level)

Chapter 1 Introduction

1.1 Context

Electricity is a vital commodity in the modern society, which requires an intensive infrastructure. In Norway each region has a grid company that operates the distribution grid in a monopolistic manner. In return, regulated by "Energiloven", the grid company is obliged to deliver power to each household in the region, with very few exceptions.[14] Many regions in Norway are sparsely populated and the coastline is long. Islands with few inhabitants require electricity supply and the options are often a connection to the national grid through long sub-marine cables or diesel generators. Sub-marine cables are expensive, and supplying the loads by a diesel generator will contribute to large CO_2 emissions.

The company TrønderEnergi Kraft are, by participating in an EU funded project, researching an alternative by implementing a microgrid. By a test facility at Rye near Trondheim they are gaining knowledge and insights on how to operate a combination of a wind turbine and solar panels with a battery and hydrogen facility in order to supply a load. A backup diesel generator will also be present. This will operate as a pilot for the technology, and the goal is to later implement this on the island of Froan. The sub-marine cable supplying these islands off the coast of Trøndelag is expected to soon require an upgrade, with an estimated cost of about 30 million NOK for 30 kilometres of cable. Installing a diesel generator is expected to be cheaper but will contribute to CO_2 emissions. This motivates the research of a renewable island operated microgrid, which will be further discussed in this thesis.[15]

1.2 Motivation

Photovoltaic solar panels and wind turbines are dependent on, among other parameters, the irradiance and the wind speed. The energy generated by these sources dictates the operation of the microgrid. However, due to the inherent intermittency of the weather dependent energy generating units, some control decisions are made on uncertain ground. In addition, the consumption of the load varies, making the required energy different per hour.

To cope with these uncertainties there has been intensive research on predicting both the output power of volatile renewable resources and of load consumption.[16, 17] This is important for both power plant owners and grid operators and has therefore seen great progress. The knowledge and experience generated by these efforts may be of importance when designing the control system of a microgrid.

Combining the need for a reliable and remote access to electricity with a goal of a renewable supply is summarized in fig. 1.1. It showcases the two lines of goals, problems and solution. This thesis aims to combine the two solutions in one management system.

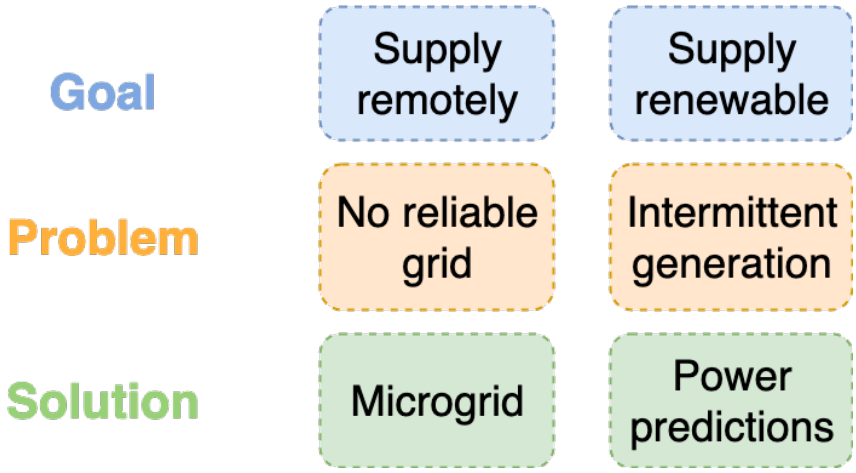

Figure 1.1: The goals, problems and solutions at hand for the thesis. The thesis combines the two solutions, microgrid and power predictions, into a new operational strategy.

1.3 Scope of work

This thesis aims to contribute in the battle to make a reliable, renewable system for remote electricity supply. It does so by designing a new operational strategy for microgrids. The hope is that it can help improve the state of the art for these solutions. The management system is to include power predictions and incorporate those when scheduling the powers of the different components. The thesis does so by conducting a case study on the Rye microgrid. The aim is to use the power of data analysis to improve the microgrid's ability to operate independently. The research will revolve around the designed management and its potential for reducing the diesel consumption. It will therefore include the following:

- **Technical description of Rye:** Discribe the technical details of the microgrid installation and derive an comprehensive overview of its components and operation.
- **Prediction models:** Apply basic machine learning models for prediction of power. The powers to be predicted are the generation from the PV- and wind installations as well as of the load at Rye.
- **Design operational strategy:** Design and implement a new scheduling logic to model the microgrid operation over a year. The control system shall take power predictions into account and optimise the power sharing.
- **Compare results to current implementation:** The current power sharing logic will also be implemented as a base case for comparison of the resulting behaviour.

1.4 Report outline

The report consists of seven chapters with the following content.

- Chapter 1 - Introduction
  This is the current chapter, which introduces some important context and terminology for the project.
- Chapter 2 - Background
  The second chapter describes the three pillars on which the rest of the thesis builds: microgrid operation, model predictive control and power predictions. It holds some general theory and brief state of the art descriptions.
- Chapter 3 - Case study: Rye Microgrid
  This chapter describes the microgrid which is to be installed at Rye, Trondheim. It contains a short technical description.
- Chapter 4 - Modelling of Microgrid Operational Control
  In the fourth chapter, the two modelling methods are explained: the base case and the predictive control. The logical foundation of the operation is described, as well as the implementation. In addition, details around the code architecture and the data on which the simulation builds are presented.
- Chapter 5 - Results
  The results are presented in chapter 5. Descriptive numbers and plots of the two operational strategies are given. They are compared to better understand the implications of different control strategies.
- Chapter 6 - Discussion and Future Work
  The sixth chapter discusses the obtained results and general weaknesses in the analysis. It also describes the work that should follow this project.
- Chapter 7 - Conclusion
  In chapter seven, the findings are summarised.

Chapter 2 Background

This chapter holds some theory necessary to understand the concepts on which this thesis is built. First, it briefly explains microgrids (MG) and microgrid operations. Then the concept of model predictive control (MPC) is briefly explained, which is the inspiration for the energy management system designed in this thesis. Lastly, an introduction to power predictions is given. Predictions of photovoltaic (PV) power, wind power and load power by machine learning (ML) is specifically described. Parts of this chapter are reused from the specialization project[18].

2.1 Microgrid operation

The concept of microgrids (MG) has been developed and elaborated on since its first occurrence. Hence, the definitions also vary accordingly. One way to define a MG is by describing it as a small, controllable power supply system that combines distributed power with loads, energy storage and control devices[19].

The intention of establishing a MG and its role in the energy system varies. It may be a part of the main grid, but operating as an entity that has inner control and is seen as one node by the utility system. In such cases it mostly operates connected to the grid but has the ability to operate independently when there is a need for it[20]. If the MG is located in a remote area where there either is no available power system or a power system of low quality and consistency, a MG may serve a different purpose. In these cases the MG is designed for island operation at all times. This makes it responsible for supplying the loads with electricity of sufficient quality without interruptions. Therefore, the dimensioning of the components, availability of storage units and control strategy is especially important.

In an islanded microgrid there are many components that must interact to obtain power balance and stable frequency and voltage levels. Three typical control architectures exist: 1) centralised, 2) decentralised and 3) hierarchical. In the centralised control, all actions are determined by a master controller. The master controller receives measurements from all involved units and determines their set points. In a decentralised control each unit has a local controller. The local controller only receives local information and based on it alters the component's behaviour. A hierarchical control is a compromise between the two.[1, 21] The centralised and decentralised control, each have their own strengths and weaknesses. An island operated microgrid usually has a fixed infrastructure and there is a crucial need to uphold a demand-supply balance, therefore a centralised or hierarchical control approach may be more suitable.[17, 22] If all the relevant information can be gathered in a common point, a centralised or hierarchical control enables the implementation of online optimisation routines.

Microgrid control often consists of three levels: I) primary, II) secondary and III) tertiary. These three levels have their own characteristics and responsibilities. An outline of their configuration is given in fig. 2.1. The primary control is the fastest control. It reacts to the dynamic behaviour of the microgrid and operates within milliseconds. It uses local measurements of voltage and current to control each unit and responds to load change. [21, 23] The secondary control represents the highest level of control within

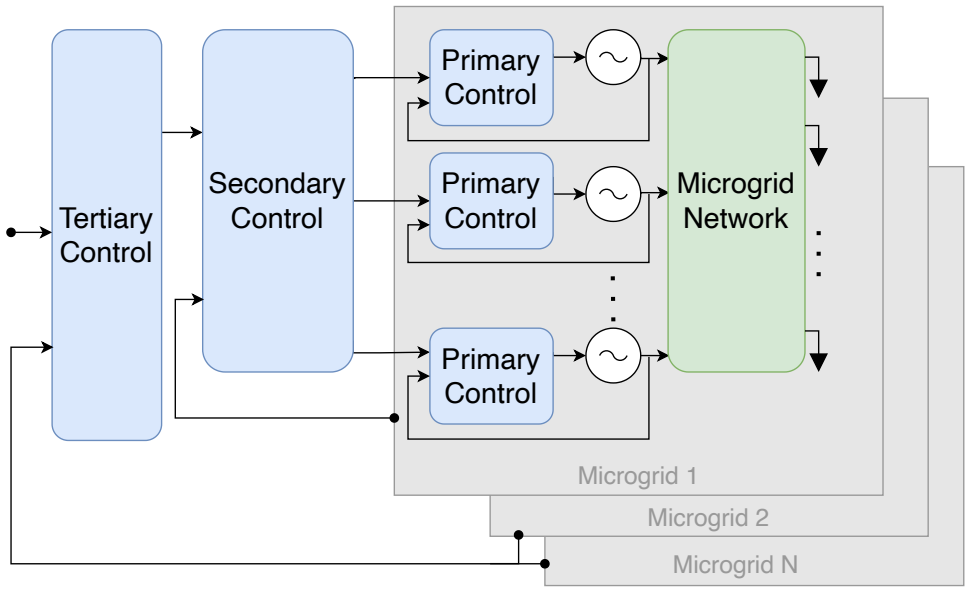

Figure 2.1: Illustration of the three levels of a hierarchical control structure. Inspired by fig 3 in [1].

the microgrid. It is slow and is responsible for making the operation secure, reliable and economical. Often, the secondary control is known as the energy management system. It determines the set points for voltage, frequency and power of the units. As the time frame is longer, the secondary control can contain more complex calculations to determine the power sharing. The secondary control is also responsible for fixing any permanent deviations or offsets, produced by the primary control.[1, 21] The tertiary control coordinates the microgrid with outside systems. This could be other microgrids or the utility grid. As this is not necessary for island operated microgrids it will not be discussed further.[1]

2.2 Model Predictive Control

The input or output power of each component in the microgrid is determined by a power sharing logic in the secondary control of the microgrid. There are many ways to determine the power sharing within the network to optimise its operation. In a centrailised or hierarchical control, Model Predictive Control (MPC) is one such method. It incorporates a cost function in order to optimise some relation in the microgrid.[21, 22, 24]

MPC has been widely used in the industry for a long period. As the computational power of microprocessors have increased, it can be utilised in more complicated and fast systems.[24, 25] It has gotten attention in the control of microgrids in recent years and several articles describe it[1, 17].

When utilised with renewable energy generation in a microgrid, the control may determine the optimal actions taking power predictions into account. The power generation and consumption over a determined horizon and with a certain time step is predicted and combined with knowledge on the microgrid. This forms the basis on which the control determines the operational state.[26] With the desired control variables predicted, the MPC minimizes a cost function in order to set the power sharing within the network.[25]

The cost function is defined to represent the desired behaviour of the system. It penalises undesired behaviour of the system or rewards desired behaviour. The design of the cost function is important and varies in each individual case, depending on the goals of the operator. It may for example penalise unmet power demand, operational costs, energy losses or component degradation.[25, 26]

2.3 Power prediction

The inclusion of power predictions in microgrid operation has been researched in recent time.[1, 17, 26, 27] Due to the natural intermittency of weather dependent renewable energies, such as PV and wind, the prediction of generation is a challenge that has been subject to intensive research. Both plant owners and grid operators will benefit from knowing the future generation from these sources. A common procedure when creating such predictions is sketched in fig. 2.2.[2] As the generation of energy is dependent on the weather, the first step is a weather forecast. This is an established science and many methods and providers exist. The output from these forecasts, such as for example the wind speed, irradiance, temperature and wind direction are utilised in the next step. A model is created to relate these weather variables to a power generation. Machine learning (ML) has in recent years gained ground for the creation of such models. This is a data driven methodology that does not require specific knowledge of the technical equipment, but rather creates a mathematical formulation based on historical data. The output from these models are a forecast of generation which can be utilised in planning and operation of the plant or grid. The power predictions done in this thesis focus on the models by ML algorithms, i.e. the orange box in fig. 2.2. [18]

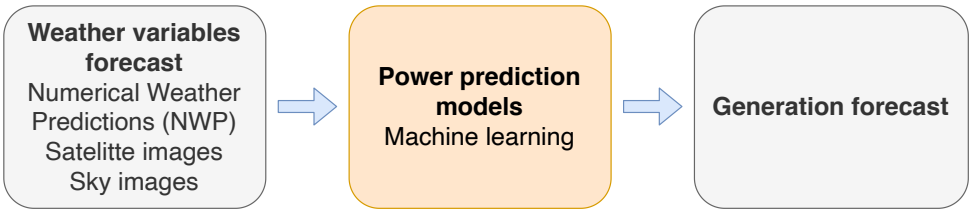

Figure 2.2: Common procedure of forecasting generation from renewable, weather dependent sources. Adapted from Fig 1 in [2].

Many different ML algorithms have been developed. One of these is the Decision Tree Regression algorithm. A decision tree is constructed recursively as outlined in fig. 2.3.

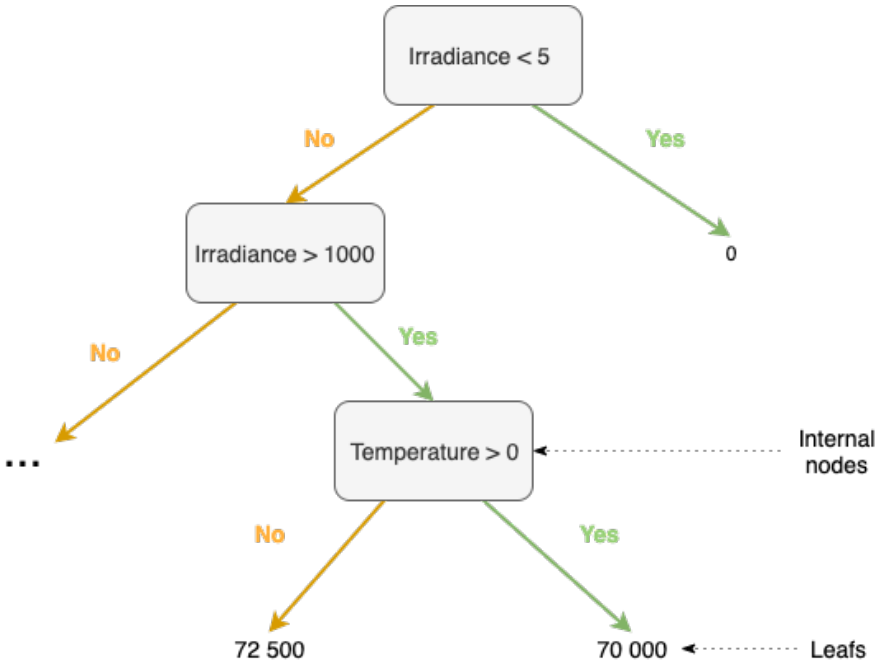

Figure 2.3: Simplified illustration of a Regression Tree. Inspired by [3].

Each node holds a true or false statement and each leaf holds a value of the target parameter or a proba-

bility function describing the outcomes at this leaf. The questions asked at each node helps the algorithm determine the value of the target parameter. The question at each node depends on the question of the above node and helps clarify a reasonable target. The splits are created based on the input data and is chosen to either minimize entropy or maximize information gain. When the split is 50/50 the entropy is maximized, and when it is 1/0, it is minimized. The difference in entropy after and before a split determines the information gain. A stopping criteria such as the depth of the tree or a stop in information gain determines when the process of creating new splits is stopped.[3, 18, 28]

There are many ways to determine the accuracy of a regression model. Different evaluation criteria have been designed to determine how close the predictions are to the real value. Three of these are the mean absolute error (MAE) eq. (2.1), the mean squared error (MSE) eq. (2.2) and the coefficient of determination (R^2) eq. (2.3).[2, 29] Here n is the total number of predictions to be evaluated, y_i is the measured value, $\hat{y}$ is the predicted value and $\bar{y}$ is the mean value.

$$MAE : \frac{1}{n}\sum_{i=1}^{n}|y_i - \hat{y}| \tag{2.1}$$

$$MSE : \frac{1}{n}\sum_{i=1}^{n}(y_i - \hat{y})^2 \tag{2.2}$$

$$R^2 : 1 - \frac{\sum_i (y_i - \hat{y})^2}{\sum_i (y_i - \bar{y})^2} \tag{2.3}$$

PV prediction

As PV panels utilise the energy in the radiation from the sun, the generated energy depends on the irradiance. In fact, the current of the panel is linearly dependent on the irradiance. In addition, the performance of the panels depend on the temperature. An increased temperature results in a decreased voltage at the panel.[30] All panels come with a coefficient for reduced performance with increased temperature. For the REC TwinPeak2, which are installed at Rye, the power is reduced with -0.37 $\%/°$C at the maximum power point.[31]

Many studies on data oriented ML models to predict solar generation have been performed.[2, 32, 33, 34, 35] All of these have in some manner utilised irradiance and temperature in their implementation. Many have also used wind speed[2, 32, 34, 35], relative humidity [2, 33, 34, 35] and wind direction[2, 34, 35]. Some have also used measurements of snow and rain[35], pressure[35] and cumulative dust[33].

Wind prediction

The power that a wind turbine may extract is known to be given by the relation in eq. (2.4). Here P_w is the output power(W), C_p is the coefficient of performance, ρ is the air mass density (kg/m^3), A is the swept blade area (m^2) and v is the wind speed (m/s). The air density is again a function of the temperature, humidity and pressure.[36]

$$P_w = \frac{1}{2}C_p A \rho v^3 \tag{2.4}$$

The parameters that, according to these relations, will determine the output power of the wind turbine is most influentially the wind speed, in addition to temperature, humidity and pressure.

Previous models created by ML therefore usually utilise wind speed as input data.[37, 38, 39, 40] Most models also use some parameters related to the air density.[38, 39, 40] In addition, some work suggests that the wind direction will also have an influence[38], as well as the power output in the previous time step, as the inertia of the turbine will create a dependency between successive time periods.[40]

Load prediction

The prediction of electric loads and their power consumption has been a hot topic of both academic and industrial research for years. The load predictions can significantly affect the operational efficiency of a power system. It can for example be utilised in unit commitment, maintenance scheduling and demand side management.[41, 42]

The load consumption varies every hour with the active appliances. When analysing one single residential load it may be extra volatile. Especially if there is power intensive equipment that has irregular time of use. This is often the case for a large farm.

However there are some parameters that tend to impact the load. These therefore make it predictable to a certain degree. When finding these relations in data driven prediction, like machine learning, historical time series data is essential. Time series of previous load values, combined with historical data on other parameters, form the basis of these models.[43] Three categories of variables may be essential when predicting the load: seasonal, environmental and social. The seasonal variations may be represented by the time of day, the week, the month or the type of day (weekday, weekend etc.). It catches the patterns of human habits over the course of time.[41, 43, 44] The environmental variations are linked to how the load changes with weather relations. Cold temperatures might for example give rise to a higher use of electric heating and high temperatures to cooling.[41, 42, 43, 44, 45, 46] And lastly the social variations may come from an increased standard of living, new equipment or new inhabitants.[41, 42]

Chapter 3 Case Study: Rye Microgrid

A microgrid is being constructed at the farm Langørgen Øvre at Rye, 12 kilometres outside the city of Trondheim, Norway. This is a test facility for the creation of microgrids as an entity for remote islands with funding from the EU program Horizon 2020.[47] This chapter is a summary of the description given in the specialisation project[18], and briefly describes the involved components.

Figure 3.1: Pictures of the microgrid being set up at Rye, Norway. Taken by Bernhard Kvaal, TrønderEnergi.

3.1 Overview

The microgrid at Rye consists of two renewable energy generating units: a wind turbine and solar panels. These are mature technologies that are well suited to supply the grid with energy. However, these sources are fluctuating and therefore balancing units for energy storage are needed. There are two main energy storage devices: a battery and a hydrogen plant (electrolyser, hydrogen tank and fuel cell). These components supply a consumer (farm load), with a diesel generator as a backup solution. Figure 3.2 shows a general overview of the system in question. Some components, as for example circuit breakers, earth connections and measurement devices, are not included.

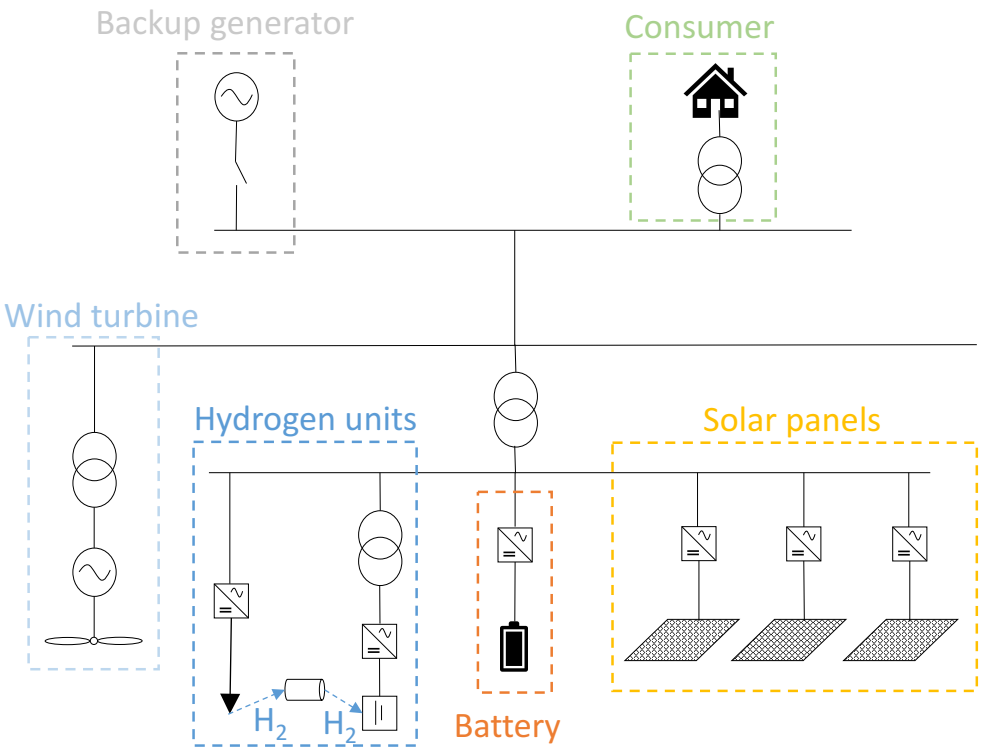

Figure 3.2: Overview of the most important components of the microgrid at Rye, excluding some technical components.[4, 5]

3.2 Wind turbine

The first energy generating unit in the system is a wind turbine of the type Vestas V27[4]. Some of the main parameters of the wind turbine are given in table 3.1, while the detailed information can be found in [10].

Table 3.1: Specifications of the wind turbine at Rye microgrid[10, 11]

Type specification	VESTAS V27, 50Hz tubular tower
Hub height	31.5 m
Rotor diameter	27 m
Generator rated power	225 kW
Generator rated voltage	400 V
Cut-in wind speed	3.5 m/s
Rated wind speed	14 m/s
Transformer efficiency	~ 0.98

The wind turbine has been in operation at Rye since 2015, when it was bought second hand from Denmark. The generation on monthly and yearly basis are pictured in fig. 3.3. In the three first years the turbine generated the most energy during the winter, which matches the general tendency in Norway.[6]

Three rotor blades are assembled on a pitch regulated rotor. From the rotor, the power is transmitted through a shaft and a two stage gearbox to the generator. The generator of the turbine is asynchronous. It has two sets of windings and can therefore operate both as a 6- or an 8 pole generator. This is to ensure that the generator can operate more optimally at different wind speeds. The generator is directly

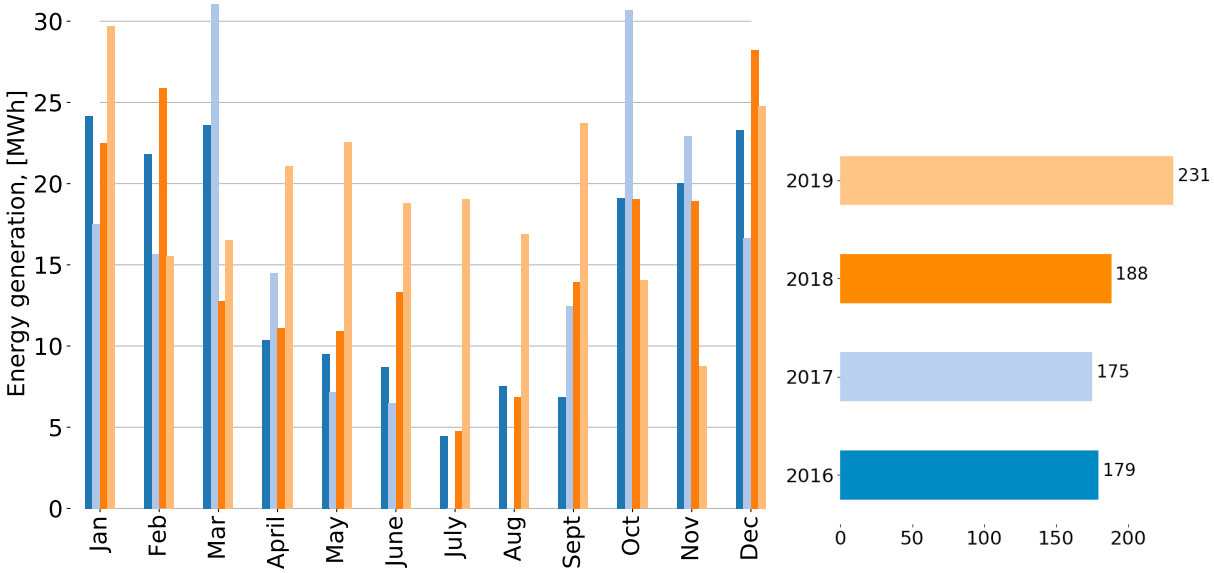

Figure 3.3: Measured monthly and yearly energy generation from wind turbine at Rye [6]. Note that the turbine was out of operation during the summer of 2017.

connected to the rest of the grid through a transformer.

3.3 Photovoltaic system

The second system for energy generation is a photovoltaic (PV) system. The panels at Rye are mounted on the ground. They are connected in nine strings combined into three inverters. Every second panel has a connected power optimiser to ensure that the maximum yield is extracted.[12] A summary of main sizes and component types are listed in table 3.2

Table 3.2: Specifications of the photovoltaic system at Rye microgrid[12].

Rated output power	86.4kWp
Rated output voltage	400 V
Panels, type	REC TwinPeak2
Number of panels	288
Power optimiser, type	SolarEdge P600/P650
Inverter, type	SolarEdge 27.6K

Several estimations on the yearly yield of the panels were done. SolarEdge estimated that the system on average would generate 87.88 MWh per year.[7] A similar estimation was done by Solbes, who estimated an annual generation of 80.36 MWh.[48] The system has been in operation since 8th of April 2019. The measurements and estimations (SolarEdge) are included in fig. 3.4. The measurements are from 30th of April 2019 to 29th of April 2020 and the estimations are those done by SolarEdge. Note that some of the measurements in December and January were lost and therefore replaced as described in section 4.4. In the course of the year it has been in operation (30/4-19 - 29/4-20) the panels generated 75.18 MWh of energy.

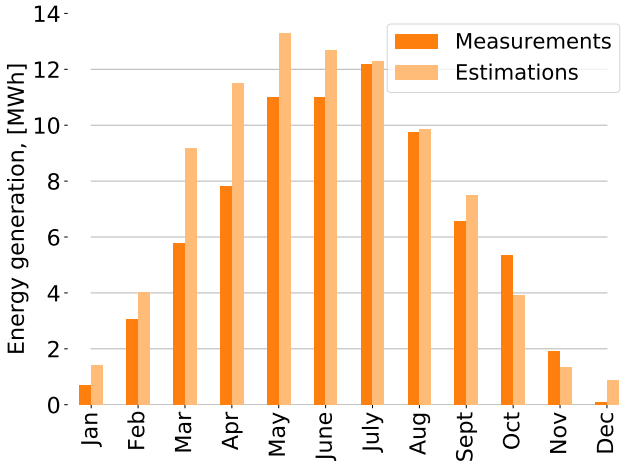

Figure 3.4: Energy generation from the solar system at Rye. Measurements from on site and estimations by SolarEdge [7].

3.4 Battery

As the energy sources are intermittent and the load fluctuating, a battery energy storage system (BESS) is installed for maintaining the balance of the system. The battery has a fast response and is therefore able to regulate the power demand and supply quickly. It is a lithium-ion battery, with key numbers listed in table 3.3. The efficiency test of the battery itself has not yet been executed, and this value therefore has some uncertainty.

Table 3.3: Specifications of the battery at Rye microgrid[5, 8]

Energy capacity (Total installed/usable)	554/500 kWh
Maximum power	400kVA
Voltage range	714-1000 V
Battery Efficiency	98%
Efficiency of DC/AC converter	98%

The battery is produced by LG Chem, one of the worlds largest manufacturers of lithium-ion batteries. Its auxillaries, control system and assembly is done by Nidec, and Powidian provides it to TrønderEnergi, who will be the final owner. The battery in the BESS at Rye contains 85 modules. These modules are connected in series of 17, constituting five racks and the total capacity is 554kWh.[9] The configuration of the battery system can be seen in fig. 3.5.

The master controller of the microgrid strives to sustain a power balance in the system. This is obtained by setting active and reactive power, P and Q, setpoints for all units in the system, except for the BESS which operates based on setpoints for voltage and frequency, V and f. The BESS is fast and is therefore able to cancel out the fluctuations in frequency and voltage in the system. With setpoints for V and f delivered from the master controller, the BESS is equipped to preserve the frequency at 50 Hz and the voltage at an acceptable level by balancing the active and reactive power.[49][18]

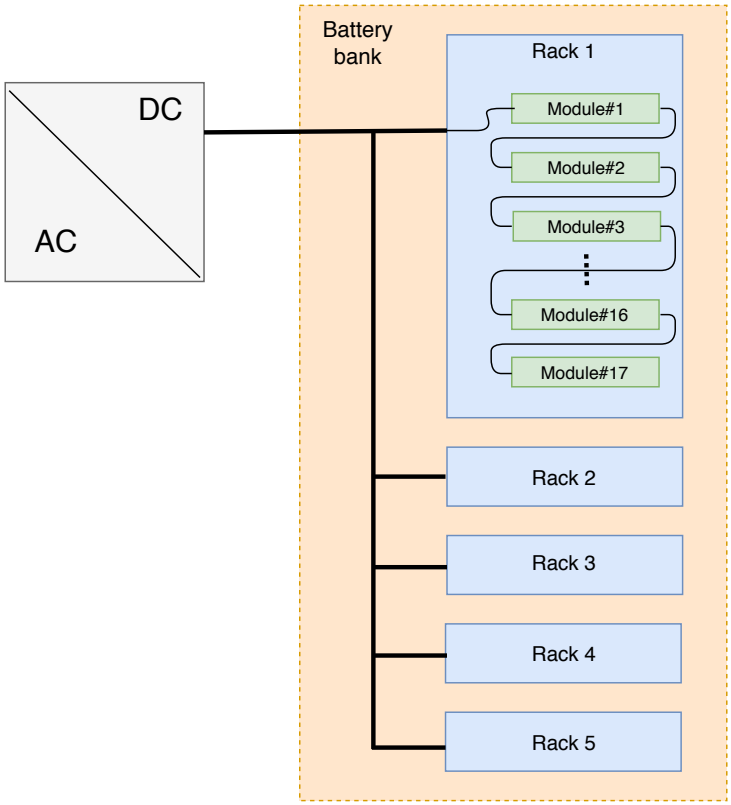

Figure 3.5: Battery system configuration. Inspired by [8]. The grey box is the inverter that connects the alternative current (AC) side of the microgrid to the direct current (DC) battery.

3.5 Hydrogen system

In addition to the BESS, there is a hydrogen energy storage system (HESS) installed in the microgrid. The HESS consists of an electrolyser with a rectifier, a hydrogen storage tank, a fuel cell with an inverter and transformer, as well as temperature regulating equipment and control- and protection units. The HESS has a slower response, but a larger storage capacity. It is therefore more suitable for the long and medium term storage. Electrolysers and fuel cells contain well-proven technology, but are still the least mature technology included in the microgrid. As hydrogen is an explosive gas, the HESS must be equipped with mechanisms to prevent explosion.

3.5.1 Electrolyser

The electrolyser can produce hydrogen to store the surplus energy provided by the renewable sources. This is done by converting electric power to hydrogen- and oxygen gas. Some of its key numbers are given in table 3.4.

Table 3.4: Specifications of the electrolyser at Rye microgrid[11]

Voltage	400V
Maximum power	55kW
Average efficiency	64.1%

The unit is connected to a rectifier which gives a DC voltage. This is combined with water to give the following red-ox reaction, where the hydrogen is stored.

$$H_2O \rightarrow \frac{1}{2}O_2 + 2H^+ + 2e^-$$

To ensure safe and efficient operation of the electrolyser its power cannot go too low. The power going into the electrolyser should be at least 20% of its maximum power. To secure ideal operation of the electrolyser, the number of starts must be minimised, as the chemical process of starting leads to wear on the system. The system will thus favour operation over longer periods compared to frequent starts.[49][9]

The electrolyser's efficiency in this process depends on the amount of power that is used. It varies as sketched in fig. 3.6 and the electrolyser will not be operated under 20% of nominal power. To secure ideal operation of the electrolyser, the number of starts must be minimised, as the chemical process of starting leads to wear on the system. The system will thus favour operation over longer periods compared to frequent starts.[49][9]

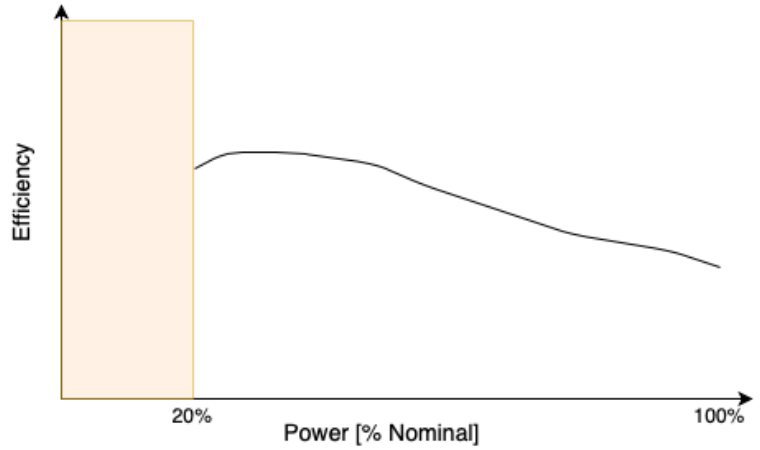

Figure 3.6: Electrolyser efficiency vs. power (% of nominal), inspired by graph in [9].

3.5.2 Hydrogen tank

The hydrogen produced by the electrolyser is fed into a pressurised tank. The container can hold 100 kg of H_2. Hydrogen has an energy density of approximately 33.33 kWh/kg [50], and the container can, therefore, store a maximum of approximately 3.3 MWh. As the fuel cell efficiency is roughly 50%, the amount of usable energy is roughly 1.67 MWh[9]. As a result, the energy storage will in practice be approximately 1.67 MWh.

3.5.3 Fuel cell

In cases of energy shortage in the MG, hydrogen is converted to electric energy through a fuel cell. The fuel cell will reverse the reaction in the electrolyser. Its most important features are noted in table 3.5. The fuel cell delivers a voltage to an inverter. The inverter is further connected to a transformer which transforms the now alternating voltage to a level of 400 V. It is of the type Proton-Exchange Membrane (PEM) fuel cell and is delivered by Ballard.[5, 9, 18]

Table 3.5: Specifications of the fuel cell at Rye microgrid[9]

Voltage	400V
Maximum power	100kW
Average efficiency	50%
Transformer efficiency	97 %
Inverter efficiency	97 %

The fuel cell efficiency also varies with the output power level. Its variation can be seen in fig. 3.7. The goal is to operate the fuel cell in the marked area of the figure, where the efficiency peaks.

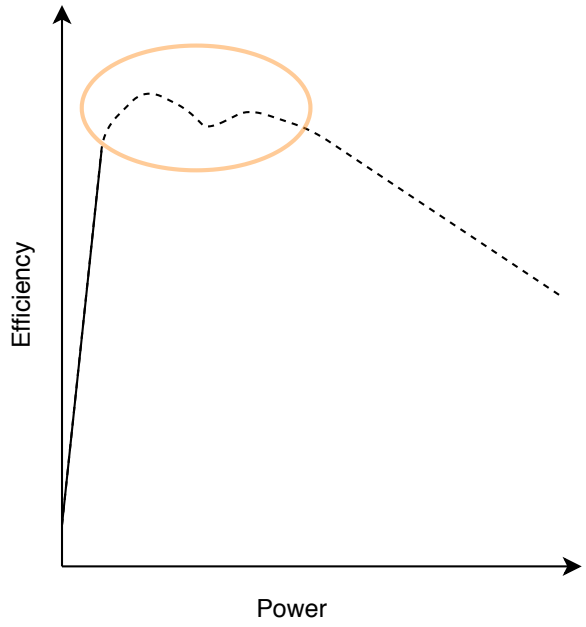

Figure 3.7: Fuel cell efficiency vs. power, inspired by graph in [9].

3.6 Load

The farm Langørgen Øvre will serve as the load in this microgrid. The farm consists of three buildings: a residential house and two barns. The microgrid was designed for an annual consumption of about 126 MWh, with an average daily consumption of 347 kWh [4]. Due to some changes at the farm the annual load has increased to about 176 MWh. The load measurements from 30th of April 2019 to 29th of April 2020 are given in fig. 3.8 and fig. 3.9.

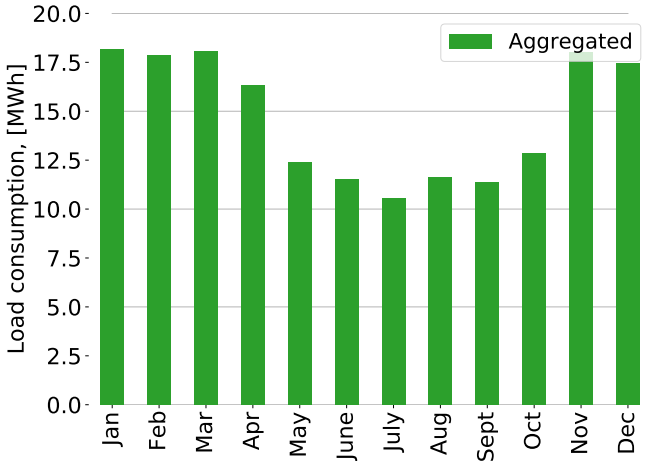

Figure 3.8: Energy consumption of load at farm 30/4-19 - 29/4/20, aggregated to monthly levels.

As can be seen in fig. 3.8 the average monthly load is between 10.5 and 18.2 MWh. There is also a seasonal variation with a high-load group (Nov-Apr) and a low-load group (May-Oct). The power demand is typically between 10 and 60 kW, with a few peaks and lows pictured in fig. 3.9. An average power demand of 20.06 kW and a peak load of 72.45 kW was found.

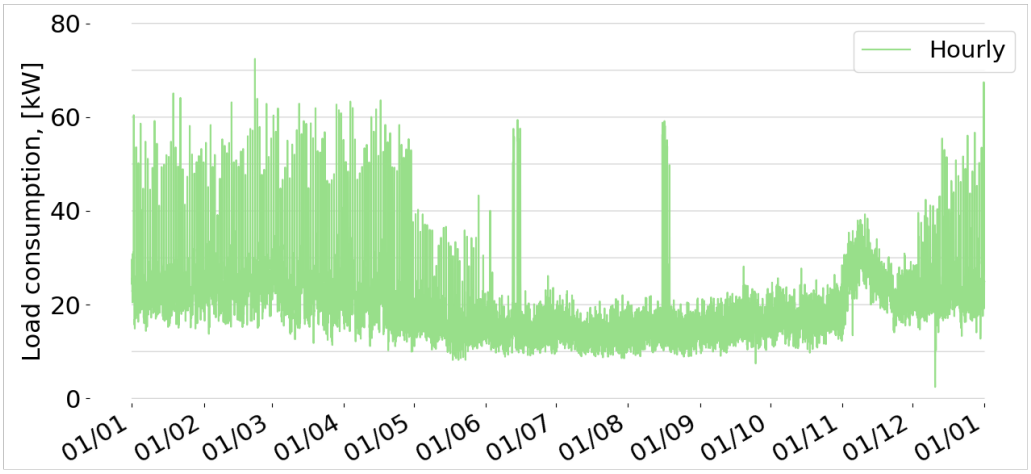

Figure 3.9: Hourly power demand at farm, 30/4-19 - 29/4/20.

3.7 Backup system

A diesel generator will be utilised as a backup for the microgrid in case of near energy shortage. This is a 66 kVA synchronous generator [13]. The peak load is approximately 96 kW, and the generator is not dimensioned to cover this load. The generator must, therefore, operate together with the energy storage systems in the MG. When the battery and hydrogen storage are beneath a given SoC, the generator will be initiated. In the current control system, the generator will then run at full power. The power from the generator will be used to supply the load, and to charge the BESS when surplus energy is available.[49]

The backup diesel generator is a synchronous generator. Before connecting it to the rest of the system, it must be synchronised with the grid. This is to avoid opposite power flow and damage of the generator. During operation, the generator will be included as a source in the control logic, and the master controller will provide it with setpoints of voltage and frequency. The generator will oversee the regulation of active- and reactive power flow in the system to maintain the desired voltage- and frequency level. The BESS will during backup operation be provided with setpoints for P and Q from the master controller.

A diesel generator is only one of several options for backup systems. MGs located close to the utility grid can utilise a direct connection to the grid as a backup. An extension of the HESS can also be an alternative. By providing the system with a hydrogen depot and an extra fuel cell, this can provide the system with backup power. For the MG at Rye, the diesel generator was considered a more robust option. This is because the MG is a pilot, being tested for the purpose of operating remotely on an island.

Chapter 4 Modelling of Microgrid Operational Control

The energy management system of the microgrid at Rye has been modelled in two ways: the currently implemented control logic (base case) and a predictive control logic. Now that the technical description of the microgrid is given, this chapter describes how these different control systems are modelled. First it describes the modelling of the base case script. Then, the modelling of the newly designed predictive control is explained. Thereafter, the code architecture of the python project is shown. And at last, the data on which the model is built and its preparation is explained.

4.1 Base case management

The energy management currently implemented in the microgrid is based on a set of rules in the master controller. The master controller in this way controls how the power flows in and out of all the involved components.

In the actual grid the control is done in real-time. The modelling on the other hand has been done on historical data per hour. The modelling of the system is based on local measurements of PV generation for every 15 minutes, wind generation for every 10 minutes and load values for every hour. These are combined to give a dataset with the temporal resolution of 1 hour. More about the datasets used may be found in section 4.4.

The logic described in this section is mainly based on a discussion with Powidian, the french company who designed the control system at Rye.[49]

4.1.1 Control logic

The master controller receives measurements from the involved components, and sends back set points. The value of these set points are determined by an inner logic. This has been modelled as seen in fig. 4.1. Time series of the three uncontrollable powers are ran through a control logic. It outputs the power in the remaining components as well as the level of storage in the battery and in the hydrogen tank.

The uncontrollable powers are the solar panel generation, P_{PV}, the wind turbine generation, P_{wi}, and the load of the farm to be supplied, P_{load}. The power that must be curtailed from the PV and the wind turbine are $P_{\text{curt, PV}}$ and $P_{\text{curt, wi}}$ respectively. From the hydrogen system the electrolyser power, P_{EL}, and fuel cell power, P_{FC}, are found, in combination with the storage level of the hydrogen tank. The battery's state of charge (SoC) and the powers of charging, $P_{\text{batt, ch}}$, and discharging, $P_{\text{batt, dch}}$, are calculated.

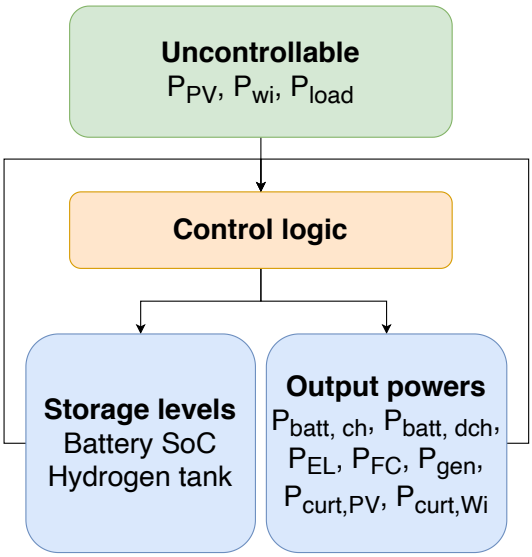

Figure 4.1: Overview of modelling of the base case control structure. Input powers in the green box, sharing logic in the orange and resulting output in the blue boxes.

The inner, orange box of control logic in fig. 4.1 is further elaborated by fig. 4.2. The values for generation and consumption combine to become the net power which can be either positive (higher generation than consumption) or negative (higher consumption than generation). Based on thresholds for the battery SoC and the hydrogen tank storage level it is decided how the power should be distributed.

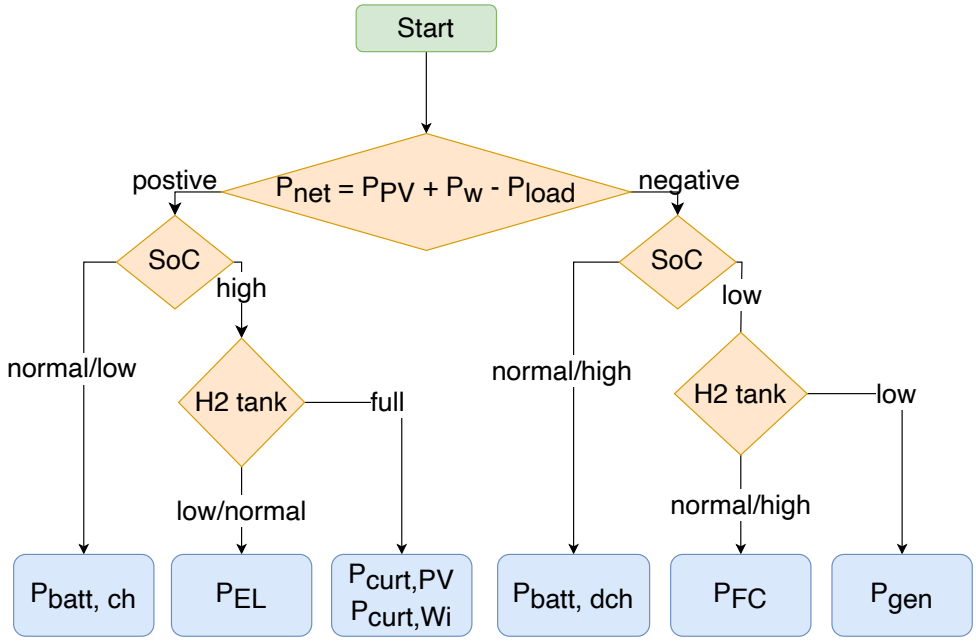

Figure 4.2: Flow chart of control logic for the base case. Elaboration of the previous figure.

This logic is executed for every hour and stored to create time series of all powers in the microgrid. Starting on the left side of the flowchart: if the net power in the grid is positive (there is excess generation), the SoC of the battery is checked. Whenever the battery is not full, the excess generation is stored by charging the battery. Should the battery be full, the hydrogen storage tank is checked. If there is room for more hydrogen, the electrolyser is started and the hydrogen stored. Should the hydrogen tank also be full, the power generation is curtailed.

If the load in the microgrid is larger than the generation, P_{net} is negative. The battery SoC is checked, and if there is a sufficient level of energy stored the battery is discharged. If the SoC of the battery is low, the hydrogen level is checked. During normal operation, with a sufficient level of hydrogen, the fuel cell is turned on. Should however the hydrogen level be low and there is no more energy in the system, the backup diesel generator is turned on.

4.1.2 Component simulation

All the technical components involved are simulated in the control system. Their technical specifications are elaborated on in chapter 3. The PV, wind and load are present at the location and in operation. Therefore their actual measurements are used. The other components are simulated to be in operation as described in this section.

PV, wind and load

The solar panels, the wind turbine and the load all have been in operation for over a year. Therefore there are sufficient measurements to use real historical data to model these components.

The PV measurements are after the inverter and therefore include all losses in the PV system. The wind turbine power measurements are taken on the low voltage side of its transformer. The efficiency of the transformer is therefore also taken into account, slightly reducing the measured power.

When there has been excess energy in the system over a period, both the battery and the hydrogen system will be full. Any generation at this point must be curtailed. In this event, the PV generation is curtailed before the wind turbine. Curtailment of the wind turbine is minimized as this may damage the pitch regulation and lead to more maintenance or quicker ageing. [49]

Battery

The battery converts electric power to chemical energy. It therefore has three parameters related to it: the charging power ($P_{\text{batt, ch}}$) and the discharging power ($P_{\text{batt, dch}}$) in kW and the battery state of charge (SoC_{batt}) in kWh.

The SoC is changed when the battery is charged and discharged and depends on the SoC in the previous timestep. The relation is as modelled by eq. (4.1). The η_{batt} is the battery efficiency including the converter.

$$SoC_{\text{batt}}(t) = SoC_{\text{batt}}(t-1) + \eta_{\text{batt}} P_{\text{batt, ch}}(t) + \frac{P_{\text{batt, dch}}(t)}{\eta_{\text{batt}}} \tag{4.1}$$

Electrolyser

The electrolyser converts electric power to hydrogen gas for storage. It is therefore modelled as the power going into the electrolyser (P_{EL}) with its average efficiency(η_{EL}).

The efficiency of the electrolyser is dynamic, and changes with the input power. The efficiency is given as kWh/kg, i.e. the amount of electric energy necessary to create one kg of hydrogen gas. The efficiency of a component is defined by the energy coming out of it in relation to the energy going in. The energy content (LHV) of the hydrogen gas, 33.33 kWh/kg, is therefore divided by the average efficiency (kWh/kg) to

get a percentwise efficiency. This results in eq. (4.2). Here η_{EL} is the electrolyser efficiency, E_{out} is the energy out of the component (hydrogen gas), E_{out} is the energy into the component (electric power), LHV_{H2} is the lower heating value of hydrogen and P_{EL} is the electric power going into the electrolyser.

$$\eta_{\text{EL}} = \frac{E_{\text{out}}}{E_{\text{in}}} = \frac{LHV_{H_2}[\text{kWh/kg}]}{P_{\text{EL}}[\text{kWh/kg}]} \tag{4.2}$$

Using eq. (4.2) the efficiency of the electrolyser is therefore as fig. 3.6. However, for the simulation, an average efficiency of 64.1% is used. The electrolyser is also limited such that it only operates at or above 20% of its nominal power.

Fuel cell

The fuel cell converts hydrogen from the tank to electrical power. It is therefore modelled as the electrical power coming out of the fuel cell (P_{FC}) with an average efficiency (η_{FC}).

The efficiency of the fuel cell is dependent on its power as in fig. 3.7. However due to necessary simplifications it is modelled as a constant average efficiency of 50.02%. The efficiency is given as the ouput electrical power compared to the hydrogen energy content in the tank (LHV). In addition to this, there are also efficiencies related to the transformer and inverter connected to the fuel cell which are included as constant efficiencies.

Hydrogen tank

The level of the hydrogen storage is influenced by the hydrogen generated by the electrolyser and the hydrogen used by the fuel cell. The content is measured in the number of kWh in terms of the LHV of the hydrogen in the tank. The level of the hydrogen in the tank is therefore given by eq. (4.3). The hydrogen tank level in the current time step is $\text{H}_2(t)$ and $\text{H}_2(t-1)$ is the hydrogen level in the previous time step.

$$\text{H}_2(t) = \text{H}_2(t-1) + P_{\text{EL}}(t) \cdot \eta_{\text{EL}} - \frac{P_{\text{FC}}(t)}{\eta_{\text{FC}}} \tag{4.3}$$

Diesel Generator

The backup diesel generator is simply simulated by its power output P_{gen}. It is set only to be used when there is little energy in both storage units. Once it has been turned on it operates as the master of the microgrid, balancing voltage and frequency levels. It is then operated at its maximum power and used to recharge the battery. This is done to ensure that there are fewer starts and stops of the generator.

4.2 Predictive control

The new, suggested control method takes predictions into account when distributing power in the microgrid. Power predictions on PV, wind and load are made with machine learning (ML) models. In each hour, the control system uses these predictions to optimise the distribution of power between the components in the microgrid. This process is further described in this chapter.

4.2.1 Predictions

For the purpose of improving the control system in the microgrid, the two weather dependent sources are predicted: the power from the solar panels (PV) and the wind turbine. Additionally the load power is predicted. The ML models are created based on local measurements at each component. The power predictions have a resolution of one hour. The python library scikit-learn[51] was used to create the models. The models are built on historical data from the site using the regression algorithm Decision Tree Regressor. The theoretical foundation for this may be found in section 2.3.

When the prediction models are created with Scikit-learn, two parameters are chosen to optimise the result: min_sample_leaf (the minimum number of samples in each leaf) and max_depth (the maximum depth of the decision tree). These were finely tuned for each dataset.

To measure the accuracy of the prediction models, the built in metrics of sklearn were used. These follow eq. (2.1), eq. (2.2) and eq. (2.3). However, the components for which the predictions are made have a different nominal power. To be able to compare the accuracy of the prediction models across components, the metrics were normalized. The attained parameters of evaluation are therefore the Normalized Mean Average Error eq. (4.4) and the Normalized Root Mean Square Error eq. (4.5).

$$nMAE : \frac{1}{P_{\text{nom}}} MAE \tag{4.4}$$

$$nRMSE : \frac{1}{P_{\text{nom}}} \sqrt{MSE} \tag{4.5}$$

PV

In [18] it was found that for the panels installed at Rye, the important values to use as input to the prediction models were: date and time, temperature and irradiance. The prediction models for the PV-panels at Rye therefore utilise $month$, day, $hour$, $irradiance$ (W/m^2) and $temperature$ ($^\circ$C) as parameters.

To train the ML model historical data should be used. However, the PV panels have only been in operation for about a year at the time of analysis. Therefore, data from the same period as the analysis had to be used for the training. This dataset is described in section 4.4. To limit the number of known data points a 50/50 split was used, such that only 50% of the data is known to the model. A min_sample_leaf of 30 and a max_depth of 20 was used.

Wind

For the wind turbine, the input parameters are chosen to be $month$, day, $hour$, $wind\ speed$, $wind\ direction$ and $temperature$ (°C).[18]

The prediction model utilised in the predictive control system is trained on data from 2018. The measurements on site from 25^{th} of September to 31^{st} of December form the foundation for the model. This resulted in a dataset of about 1 790 hourly data points as some measurements were absent. Of these data points, 80 % were used for training and 20% for testing. A min_sample_leaf of 5 and a max_depth of 20 was used.

As little on the wind turbine itself has changed since 2018, a model trained on this subset is expected to yield a fairly descriptive model. Since the turbine has been in operation for a while there is a rather substantial amount of data. However, as the data points used for training only cover about three months of a year some seasonal behaviour cannot be described.

Load

For the load prediction only the timing of the measurement is taken into account. By doing so, the model attempts to find a repeating pattern in the load profile. The input parameters are thereby $month$, day and $hour$.

The measurements on the farm is done by several measurement devices and systems. Some only save hourly values for three months, while others do so for the whole history. In addition, some new installation of heating equipment and new residents on the farm make the old data outdated. The prediction model was therefore trained on the same data used in the simulation. This dataset is descrbed in section 4.4. It contains about 8780 hourly values, of which 50% is used for training and 50% for testing. This is done to reduce the amount of data points that were used for both training and simulation.

4.2.2 Implementation

The control system modelling was done by creating a rather large python project. This section aims to describe how the predictive control system was implemented. An overview flow chart of the predictive control implemented is given in fig. 4.3. This is heavily inspired by the Model Predictive Control, briefly described in section 2.2.

- Before the control simulation can begin, the characteristics of the system is set. The architecture surrounding the modelling is also set in place. Now the control modelling may begin.
- First, predictions on the desired control variables of the systems are made. These are done based on weather parameters, for as many hours as the control horizon.
- Second, these predictions are used in the optimisation algorithm. By minimizing the cost function a series of control actions are generated which optimise the operation.
- Then, the first time step in the optimisation result is applied by the controller. Any errors in predictions must be accounted for and re-balanced when actions are applied to the system.
- The process is repeated until all hours are covered.

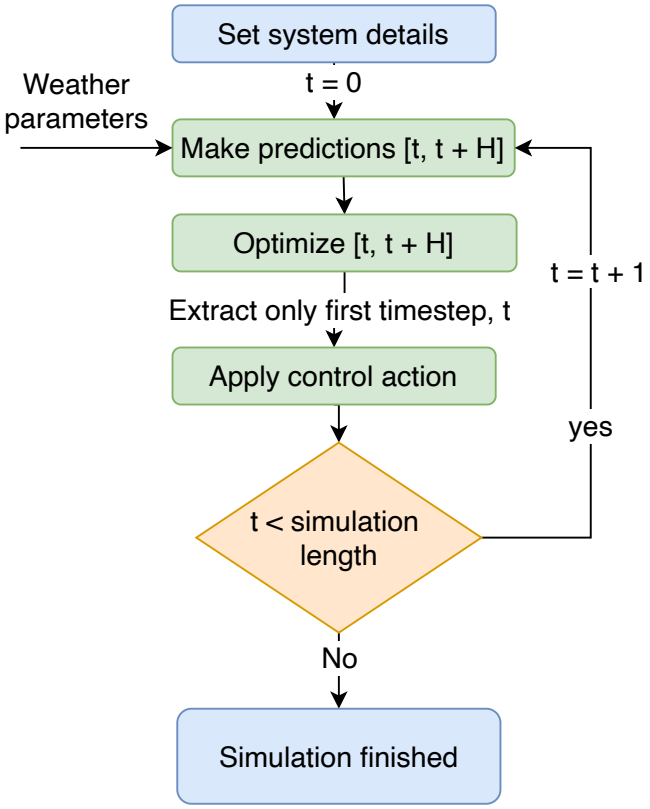

Figure 4.3: General description of the predictive control algorithm. The current time step is denoted t, while H is the contorl horizon.

In this way the sequence of tasks is completed in each sampling time and generates a series of control actions. In each time step only the first control action is applied before the process is repeated and new, optimised actions are generated.[25]

The predicted variables, $\mathcal{P}(t)$, are predicted from the current time step, k, until the defined control horizon H. The simulations executed in this thesis were mainly with a control horizon of 24 hours, but this is a flexible parameter. This results in the following H predictions.[25]

$$\mathcal{P}(t) = [\mathcal{P}(k), \mathcal{P}(k+1) \dots \mathcal{P}(k+H)] \tag{4.6}$$

The variables to be determined by the optimisation problem are the powers of each component in the MG. These are noted, P_{i}, and are as described in eq. (4.7).

$$P_i \in [P_{\text{PV}}, P_{\text{wi}}, P_{\text{EL}}, P_{\text{FC}}, P_{\text{batt, ch}}, P_{\text{batt, dch}}, P_{\text{load}}, P_{\text{gen}}] \tag{4.7}$$

They are related to the components as pictured in fig. 4.4 and are defined positive in the direction given in the figure.

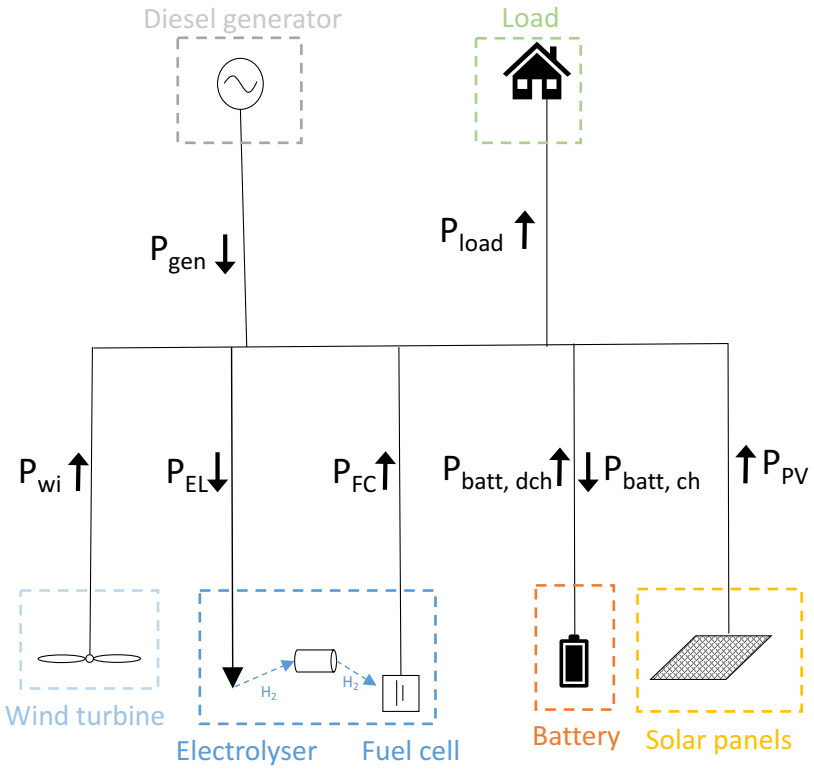

Figure 4.4: An overview of the microgrid and all the simulated powers. The direction of the arrow defines the positive direction.

Optimisation

The optimisation of the involved component powers is executed in every timestep. It is done through the Pyomo framework in Python.[52, 53] The Gurobi solver is used for solving the constructed optimisation problem.[54]

The objective function may be seen as the heart of the optimisation. It determines what is good and what is bad behaviour. In this microgrid implementation it balances several purposes. It is therefore the combination of multiple functions.

The most important goal of the microgrid at Rye is keeping the station in island operation mode. That means making sure that the renewable resources and storage components can serve the load alone. A clear goal from TrønderEnergi is to keep the usage of the diesel generator to less than 5%. This is why minimizing the diesel generator usage is the most important component of the objective function.

$$f_{\text{gen}} = \sum_{t=k}^{k+H} P_{\text{gen}}(t) \tag{4.8}$$

As the optimisation has a limited control horizon its capabilities of handling seasonal variations is low. Therefore, to ensure the adequate level of energy in the storage units, the energy curtailment must be minimized. All energy is better stored in the balancing units than not being produced. The curtailed energy, as seen by the optimisation algorithm is given by eq. (4.9)

$$f_{\text{curt, PV}} = \sum_t \mathcal{P}_{\text{PV}}(t) - P_{\text{PV}(t)} \qquad f_{\text{curt, wi}} = \sum_t \mathcal{P}_{\text{wi}}(t) - P_{\text{wi}(t)} \tag{4.9}$$

In all conversion processes between components there is a loss. This is also the case for the battery, where losses occur both in the converter and in the battery itself. The losses are given by the relation in eq. (4.10). In addition to energy loss, an overly eager use of the battery may lead to degradation of the components. To limit unnecessary conversion, these losses are included in the objective function.

$$f_{\text{batt}} = (\frac{1 - \eta_{\text{batt, dch}}}{\eta_{\text{Batt,dch}}}) \cdot \sum_{t=k}^{k+H} P_{\text{batt, dch}}(t) + (1 - \eta_{\text{batt, ch}}) \cdot \sum_{t=k}^{k+H} P_{\text{batt, ch}} \tag{4.10}$$

Losses of energy also occur in the hydrogen components. Both in the main components, the electrolyser and the fuel cell, as well as in the surrounding conversion system. The descriptive relation is given by eq. (4.11). As these are chemical components, they are especially vulnerable to degradation and limiting their usage is therefore important.

$$f_{\text{H2}} = (\frac{1 - \eta_{\text{FC}}}{\eta_{\text{FC}}}) \cdot \sum_{t=k}^{k+H} P_{\text{FC}}(t) + (1 - \eta_{\text{EL}}) \cdot \sum_{t=k}^{k+H} P_{\text{EL}}(t) \tag{4.11}$$

The final objective function is a combination of the three functions described above. This results in the objective function described in eq. (4.12). The numbers a, b, c, d and e are weighting factors to balance the importance of each component of the objective function. Having these weighting factors enables parts of the objective function to be left out, by setting them to zero. It also makes the control system dynamic to quickly alter the behaviour of the system. These were found by testing their implication on the performance of the control system. Tests with different weighing factors over the course of 1500 simulation hours were executed.

$$f_{\text{obj}} = a \cdot f_{\text{gen}} + b \cdot f_{\text{batt}} + c \cdot f_{\text{H2}} + d \cdot f_{\text{curt, PV}} + e \cdot f_{\text{curt, wi}} \tag{4.12}$$

All powers listed in eq. (4.7) are constrained by the technical characteristics of the individual components. The lower bound being l_{b} and the upper bound being u_{b}.

$$P_{\text{i}} = \{l_{\text{b}}, u_{\text{b}}\} \tag{4.13}$$

The components where power predictions exist, have the predicted power as their upper bound. This is because the power that can be extracted from the panels and the turbine is not their technical maximum. The maximum available power from these components depend on other factors, such as the weather. The load is bounded both upwards and downwards by its prediction, this is because the load must be met and there is no flexibility. The others are limited by their given maximum power. The resulting bounds of the components are given in table table 4.1.

Table 4.1: Lower and upper bounds of power variables.[13][8][9]

Variables	Lower bound (l_b)	Upper bound, (u_b)
$P_\text{PV}(t)$	0	$\mathcal{P}_\text{PV}$
$P_\text{wi}(t)$	0	$\mathcal{P}_\text{wi}$
$P_\text{load}(t)$	$\mathcal{P}_\text{load}$	$\mathcal{P}_\text{load}$
$P_\text{batt, ch}(t)$	0	400 kW
$P_\text{batt, ch}(t)$	0	400 kW
$P_\text{EL}(t)$	0	55 kW
$P_\text{FC}(t)$	0	100 kW
$P_\text{gen}(t)$	0	53 kW

Certain powers should not be active at the same time. The battery should not charge and discharge at the same time, and the electrolyser and fuel cell should not be active in the same hour. Binary variables are therefore included for each of these components. This results in four binary variables as in eq. (4.14).

$$\delta_i \in [\delta_\text{batt, ch}, \delta_\text{batt, dch}, \delta_\text{FC}, \delta_\text{EL}] \qquad \delta_i = [0, 1] \tag{4.14}$$

The binary variables are constrained as in eq. (4.15). In all constraints that include the power of these components the corresponding binary is multiplied. In this way they can never be on at the same time.

$$\delta_\text{batt, ch} + \delta_\text{batt, dch} \leq 1 \qquad \delta_\text{EL} + \delta_\text{FC} \leq 1 \tag{4.15}$$

As mentioned in section 3.5.1, the electrolyser cannot operate below 20% of nominal power. The electrolyser power variable is therefore a semi-continuous variable. By adding a constraint like in eq. (4.16) it is ensured that the electrolyser either is turned off ($P_\text{EL} = 0$) or operates in the range 20-100% of nominal power.

$$P_\text{EL} = \{20\% \cdot u_\text{b} \cdot \delta_\text{EL}, u_\text{b} \cdot \delta_\text{EL}\} \tag{4.16}$$

The levels of energy in the battery and hydrogen tank are simulated. These variables are dependent on the value in the previous time step, the value of the related power and the component efficiency as in eq. (4.17) and eq. (4.18). As the powers are always given in hourly values, the powers in kW can be added straight to the energies in kWh.

$$SoC(t) = SoC(t-1) + \eta_\text{bat} P_\text{batt, ch}(t) \cdot \delta_\text{batt, ch} + \frac{P_\text{batt, dch}(t) \cdot \delta_\text{batt, dch}}{\eta_\text{bat}} \tag{4.17}$$

$$\text{H}_2(t) = \text{H}_2(t-1) + P_\text{EL}(t) \cdot \delta_\text{EL} \cdot \eta_\text{EL} - \frac{P_\text{FC}(t) \cdot \delta_\text{FC}}{\eta_\text{FC}} \tag{4.18}$$

Storage level bounds are also in place, as described by eq. (4.19). The battery charging and discharging rate becomes limited when the battery SoC is too low or too high. In addition, as the battery is responsible for the dynamic response (voltage and frequency regulation) its energy level cannot go too low. It is

therefore limited to minimum 10% of total storable energy and maximum 90%. The hydrogen tank is operated in the range 1-98% of maximum levels.

$$SoC(t) \in [55.4, 500]\text{kWh} \qquad \text{H}_2(t) \in [33, 3234]\text{kWh} \tag{4.19}$$

All the powers in the grid must be in balance in order to obtain a stable frequency. Therefore, a power balance constraint is in place. It combines the numerical power variables and binary variables of all the included powers.

$$P_{\text{batt, dch}} \cdot \delta_{\text{batt, dch}} - P_{\text{batt, ch}} \cdot \delta_{\text{batt, ch}} - P_{\text{EL}} \cdot \delta_{\text{EL}} + P_{\text{FC}} \cdot \delta_{\text{FC}} + P_{\text{Gen}} + P_{\text{PV}} + P_{\text{wi}} - P_{\text{load}} = 0 \tag{4.20}$$

Apply control action

When the optimal scheduling of powers between the components has been found, the set points must be sent to the involved components. However, the optimised scheduling was created with the predicted values of the PV, wind and load powers. When applied, the real values might differ. The surplus or deficit of the defined schedule is therefore found by eq. (4.21). The real power delivered by the solar panels in this time instant is given by $P_{\text{PV, real}}$. The actual power from the wind turbine is $P_{\text{wi, real}}$, while the real load value is $P_{\text{load, real}}$.

$$\begin{aligned} surplus/deficit = P_{\text{batt, dch}} - P_{\text{batt, ch}} + P_{\text{FC}} - P_{\text{EL}} + P_{\text{gen}} + P_{\text{PV, real}} + P_{\text{wi, real}} + P_{\text{load, real}} \\ - P_{\text{PV, curt}} - P_{\text{wi, curt}} \end{aligned} \tag{4.21}$$

This (hopefully) small amount of power will be distributed according to the logic described by fig. 4.5.

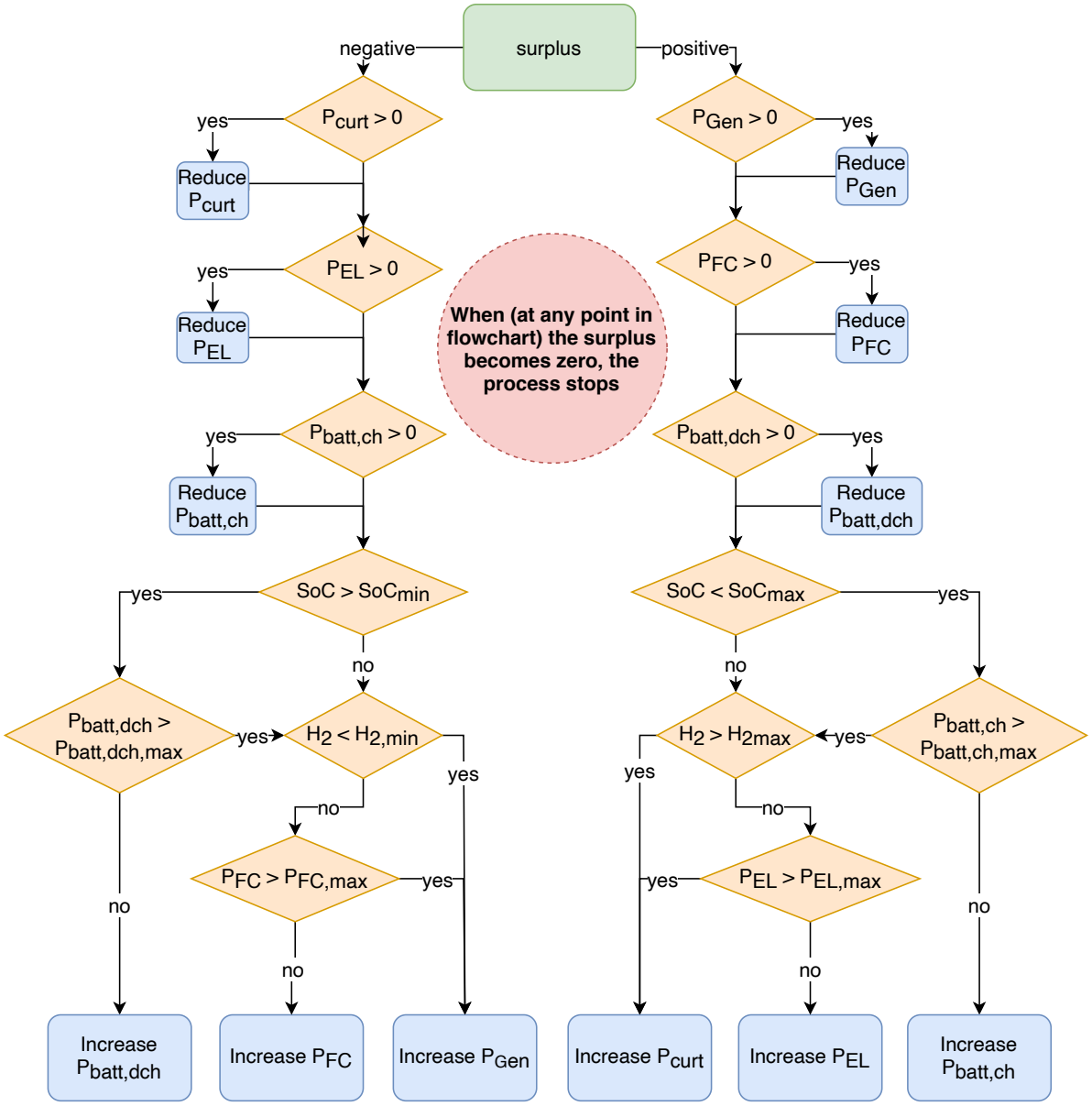

Figure 4.5: Flow chart of the implemenation of applying the control action. It describes the balancing of the power difference between optimised and real available powers.

4.3 Code architecture

Now that the theoretical concepts of implementation are described, this section gives an overview of the technical details of implementation. It describes how the different files are organized to constitue the project. It thereafter gives a brief pseudocode to better understand the code, before a section on the robustness of the code. Finally there is a section describing the data preparation that took place.

4.3.1 File hierarchy

One large folder contains all the relevant files to perform the simulation, both the base case and the predictive control modelling. This section briefly describes its content and function. The overview of the file hierarchy is given in fig. 4.6.

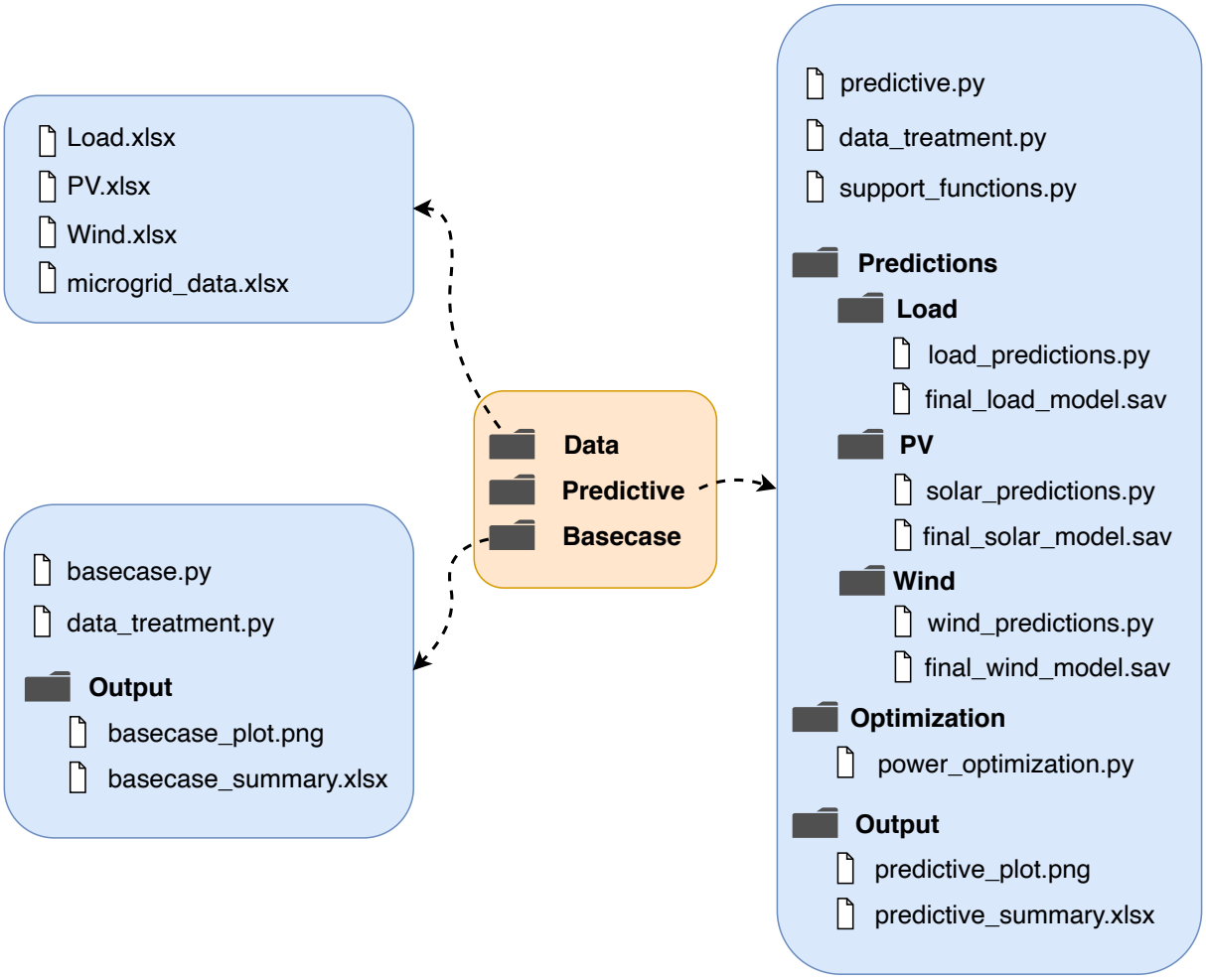

Figure 4.6: File hierarchy of the simulation. These files hold everything necessary for modelling both control systems of the microgrid. The orange box holds the main folders, and the blue boxes the relevant subfolders.

The $Data$ folder contains hourly measurements from the components installed on-site at Rye as well as the technical specifications of all involved components. More details on the data utilised may be found in section 4.4. The files in this folder are important for the function of all the rest of the simulations. The time series in $Load.xlsx$, $PV.xlsx$ and $Wind.xlsx$ lay the foundation for simulations in both the base case and in the predictive control. They contain the hourly power values of the components, as well as measurements of for example irradiance and wind speed utilised in the predictions. More details on which parameters are used for the predictions may be found in section 4.2.1. The file $microgrid\_data.xlsx$ contains information on maximum and minimum levels for component powers and storage levels, as well as efficiencies. By having one central location for all this data, the system becomes more dynamic and robust. Throughout the code, whenever such a number is utilised, it is gathered from this file. This makes it easy to alter the numbers in the simulation to make adaptions. It also makes it easier to utilise the designed control system on a different microgrid later.

The $Basecase$-folder contains a simulation of the currently implemented control at Rye. To the best of the authors ability it describes the energy management logic currently in place. The $basecase.py$ is a script which executes the controller logic according to the explanations in section 4.1. Functions realted to input- and output data treatment is stored in $data\_treatment.py$ while the output data is stored in the $Output$-folder.

One of the main contribution of this thesis is the design of the predictive control system stored under the folder $Predictive$. The operational principle of the system is described by fig. 4.3. The simulation is started by running the $predictive.py$ file. This contains the skeleton of the simulation and calls functions from other files throughout the $Predictive$-folder.

4.3.2 Pseudocode

How the simulation is executed is described by fig. 4.7. The different function calls within the $predictive.py$-file are listed with their origin and oreder. Many detailes have been left out of this figure, but the concept should be covered.

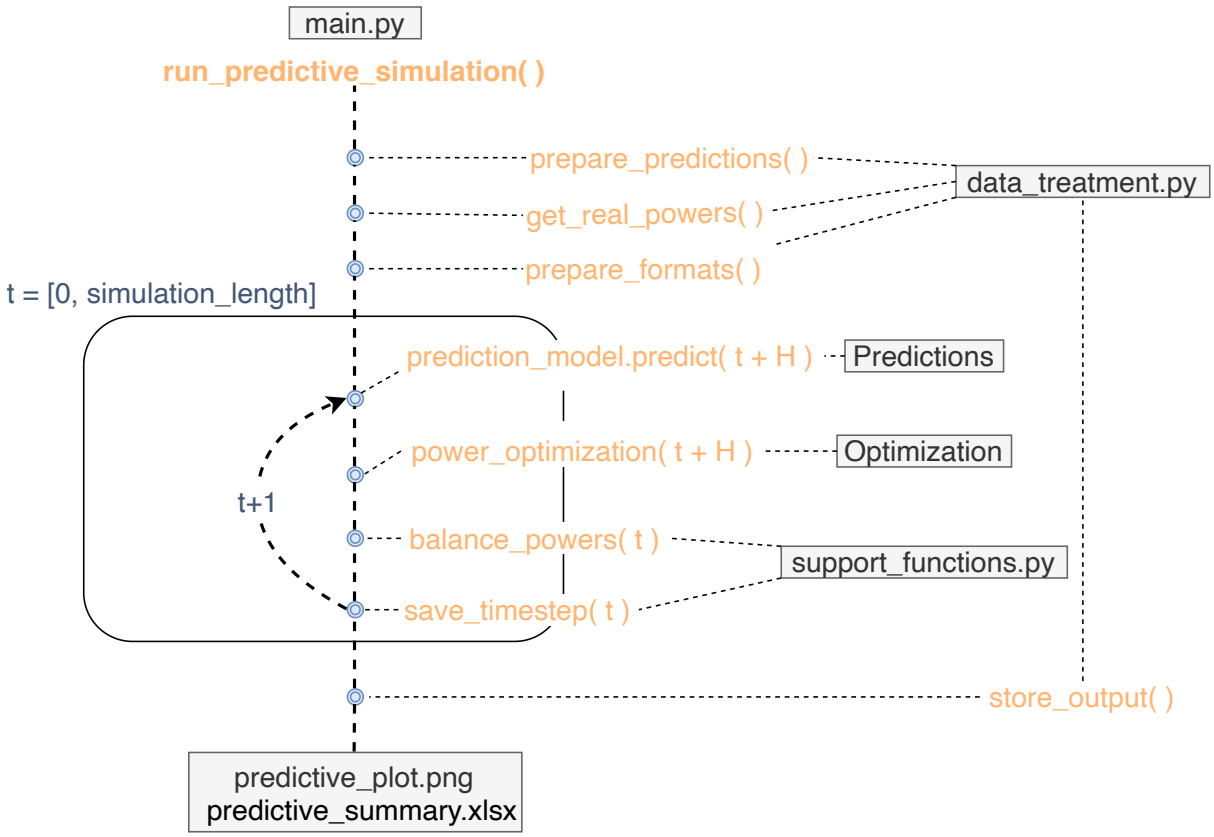

Figure 4.7: Implementation of the predictive control and the relations between the different nodes. The orange texts are functions, the grey boxes are folders or files and the blue circles are function calls. The current time step in the simulation is t, while the control horizon is denoted H.

First there are some preparations in order to make storage formats and retrieve information from other files. This is mainly done by functions in the $data\_treatment.py$-file. Then the loop which goes over all $t's$ in the simulation_length starts. The simulation is ran over one year, approximately $t = 8760$ h, but the amount of hours is flexible according to the length of the time series in the $Data$-folder. For each time step, all the functions within the box are executed. The three powers of wind, PV and load are predicted. These are then taken as input into the power optimisation. From the result of the optimisation, the powers are applied to their components. This is done by balancing the powers again when the powers are a fact and not a prediction. Then the designated powers are saved for that timestep. Lastly, when all time steps are simulated, the results are saved to a plot and a summary file.

4.3.3 Code robustness

As the constructed model is designed to control the operation of the microgrid, it is vital that it does not fail. The optimisation model is sensitive, and even if it should not fail, it some times can. The microgrid is responsible for supplying electricity to its customers and cannot afford downtime. During most hours of operation, the scheduling of powers is done according to the description in the previous section. However, should there be an error in the optimisation, a backup solution is constructed. This is described by fig. 4.8.

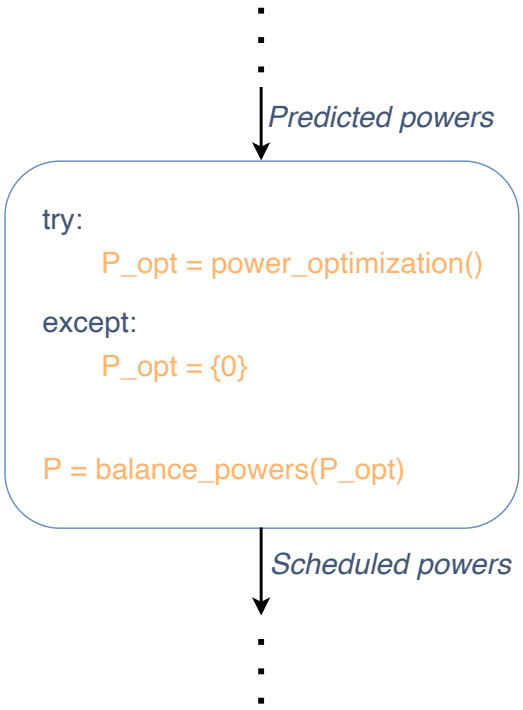

Figure 4.8: Conceptual sketch of the backup solution to ensure code robustness.

During all normal operations, the code executes the optimisation by running the $power\_optimisation()$-function in the try-block. Should the optimisation, for some reason, throw an error, the $except$-block is executed. The generating unit and load powers are set to their predicted powers, and all other powers to zero. Then, independently of the previous action the $balance\_powers()$-function is activated. This holds the logic explained in section 4.2.2. By doing so, the $balance\_powers()$-function acts both as previously described and as a backup solution.

4.4 Data preparation

This project relies on hourly measurements from three components at the microgrid at Rye. From the wind turbine, the generated power, wind direction, wind speed and temperature is used. The generated power, irradiance and temperature is gather from the solar panels. And from the farm load, the consumed power is recorded.

These values are recorded on site by different measuring devices and stored in different storage solutions. This lead to issues with data not being stored long enough and points in the dataset being gone. This section therefore describes the steps taken to achieve a coherent dataset of all the necessary values.

The final dataset covers an entire year on an hourly basis. As the measurements had different availability it is not one calendar year, but a year comprised of data from 2019 and 2020. When the simluations are run, the dataset is built such that it starts with 2020 values and values from 2019 follow. This makes the simulation follow the calendar months from January until December.

Table 4.2: The dates from which the different data is gathered by each component.

Component	Dates covered
PV	30^{th} of April 2019 - 29^{th} of April 2020
Wind	25^{th} of March 2019 - 25^{th} of March 2020
Load	30^{th} of April 2019 - 29^{th} of April 2020

Load

The load on the farm supplied by the microgrid is a combination of several buildings. The load within these buildings are measured by different systems.

The main load of the farm is measured by an eGauge system and is stored for all relevant hours. These are used directly and make up the largest part of the load.

However, the load in a different pig barn is measured by a Smappee system. This hourly consumption data is only saved for three months. When collecting historic consumption data it was found that only data from February, March and April 2020 was available for this circuit. The monthly average was, however, available for all months over the last year. Consumption levels for the previous months was thereby produced based on the consumption profile from March 2020 multiplied with a factor found based on the monthly average. The monthly average and the factor used can be found in table 4.3. This results in a pattern with reasonable hourly variations altered for seasonal differences.

Table 4.3: Monthly average consumption and factor multiplied with data from March to generate consumption data from the circuit by the pigs barn.

Month	Monthly average power [kW]	Factor
January	2.394	1.257
February	-	Original data used
March	-	Original data used
April	-	Original data used
May	1.230	0.645
June	1.621	0.851
July	1.764	0.926
August	1.941	1.019
September	1.248	0.655
October	0.629	0.330
November	2.055	1.079
December	2.173	1.140

PV

The data from the solar panels is collected through SolarEdge's monitoring system. It records all the necessary parameters for the simulation period. However, due to work on installing the microgrid some datapoints were lost. These therefore are replaced by other methods. Details on all altered data points for the PV system are given in the Appendix.

In the period 6/12-19 1:00 - 9/1-20 1:00 all datapoints were absent. From the simulations that are available at renewables.ninja, replacements were generated.[55] The available parameters were tweaked until the generation output was similar to those recorded by SolarEdge at Rye in other months.

Wind

The wind measurements were made with 10 minute intervals, all on the wind turbine. To make a coherent datasets several measurements had to be fixed. First, all duplicates were removed. Thereafter, all the datapoints were analysed to replace missing values. When the missing values covered a time less than four hours, they were replaced by a linear function between the previous and coming data points. With gaps larger than four hours the values were replaced by the values of the previous day. Thereafter all the 10 minutes measurements were averaged in order to make up an hourly dataset. Details on all the altered wind data points are given in the Appendix.

Chapter 5 Results

5.1 Base case

This report is among the first to have made simulations of the microgrid including real time measurements of all the generating units and the load. Therefore, this section aims to evaluate some key numbers found in the base case simulation.

5.1.1 Power balance

The total power generation and consumption in the microgrid are given in eq. (5.1). During previous design evaluations the total renewable power generation was found to be 284.68 MWh and the load 126.75 MWh.[5] Both evaluations therefore find that there is a power surplus, but the sizes differ. Especially the increase in yearly load is significant. When the total generation also is lower, it is expected to give rise to issues in the energy balance of the microgrid. The hourly power values over the year are given in fig. 5.1.

$$E_{\text{PV}} = 75.18\text{MWh} \qquad E_{\text{Wind}} = 190.56\text{MWh} \qquad E_{\text{Load}} = 176.18\text{MWh} \tag{5.1}$$

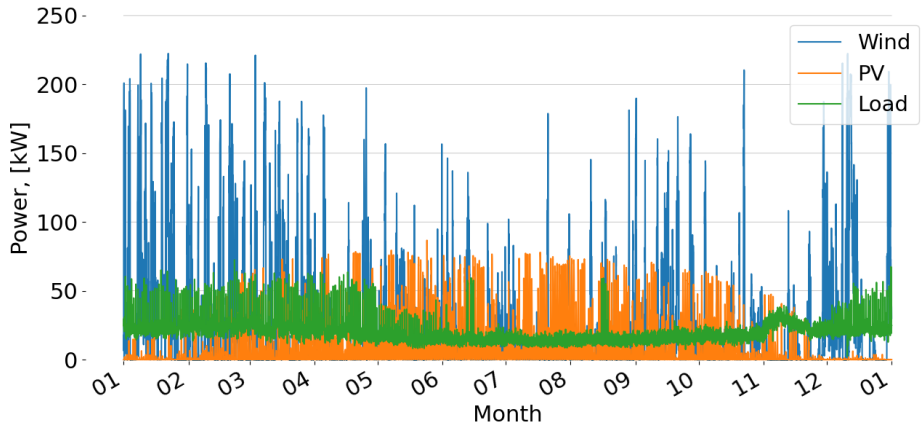

Figure 5.1: Input powers of the system. The generation of PV and wind and the load of the system on an hourly basis.

5.1.2 Component utilisation

To begin to understand how the microgrid is operated the plots in fig. 5.2 show when the different components are operated. It shows that the battery is operated very frequently, both by charging and discharging. This is accodring to the expectations as the battery is the fast acting storage solution to balance hourly imbalances. The hydrogen components (EL and FC) are operated less frequently. The hydrogen components are also vital and are used alternatively. An important note is how for the entire summer (May-mid August) the fuel cell is not used. This indicates the power surplus that is a result of the large PV generation and lower load. The generator is also forced to be active in certain hours during November-Mid April. This is the deficit period of the microgrid, and the generator usage should be limited.

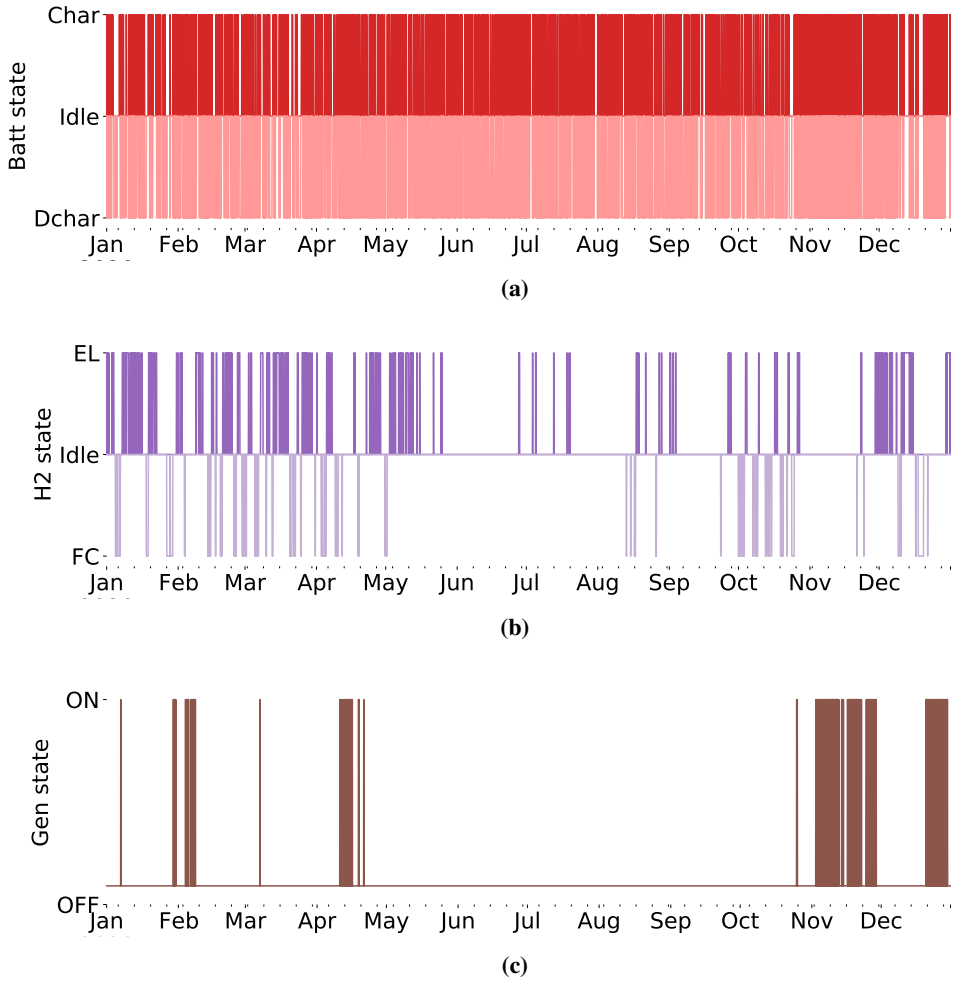

Figure 5.2: Base case hourly states of the different components. (a) Battery states. Charging, discharging and idleness. (b) Hydrogen states. Electrolyser, fuel cell and idleness. (c) Generator states. ON and OFF.

The plots in fig. 5.2 only show in which hours the different components are active. To get a grasp of how the powers are distributed within the grid on a numerical scale is important. To get a sense of this, the powers in all hours of the year, $P_{i,t}$ are summarised per component. This gives the total energy per component E_i. These are combined as in eq. (5.3), eq. (5.4) and eq. (5.2) to give a better insight. As evident, the battery is the most important component. The fuel cell covers a certain amount of the power, but not very large. When the microgrid was designed, it was meant to be 95% independently off-grid and renewable. The diesel coverage of 13.45% is high.

$$\text{Diesel coverage} = \frac{E_{\text{Gen}}}{E_{\text{load}}} = \frac{54.08\text{MWh}}{176.18\text{MWh}} = 13.45\% \tag{5.2}$$

$$\text{Battery coverage} = \frac{E_{\text{batt, dch}}}{E_{\text{load}}} = \frac{54.08\text{MWh}}{176.18\text{MWh}} = 30.70\% \tag{5.3}$$

$$\text{Fuel cell coverage} = \frac{E_{\text{FC}}}{E_{\text{load}}} = \frac{12.76\text{MWh}}{176.18\text{MWh}} = 7.24\% \tag{5.4}$$

As not all energy generated by the solar panels and the wind turbine can be stored, some is also curtailed. To get a sense of the scale of this, the curtailed energy as a percentage of the total load energy is given in eq. (5.5) and eq. (5.6).

$$\text{PV curtailment} = \frac{E_{\text{Curt, PV}}}{E_{\text{PV}}} = \frac{18.55\text{MWh}}{75.18\text{MWh}} = 24.67\% \tag{5.5}$$

$$\text{Wind curtailment} = \frac{E_{\text{Curt, Wi}}}{E_{\text{Wi}}} = \frac{85.43\text{MWh}}{190.56\text{MWh}} = 44.83\% \tag{5.6}$$

The energy level in both storage solutions vary over the course of the year. This can be seen in fig. 5.3. Again it can be seen that the battery has the most frequent variations. The hydrogen tank takes the seasonal deviations. The surplus of energy during the summer results in a full hydrogen tank from mid May to the beginning of October.

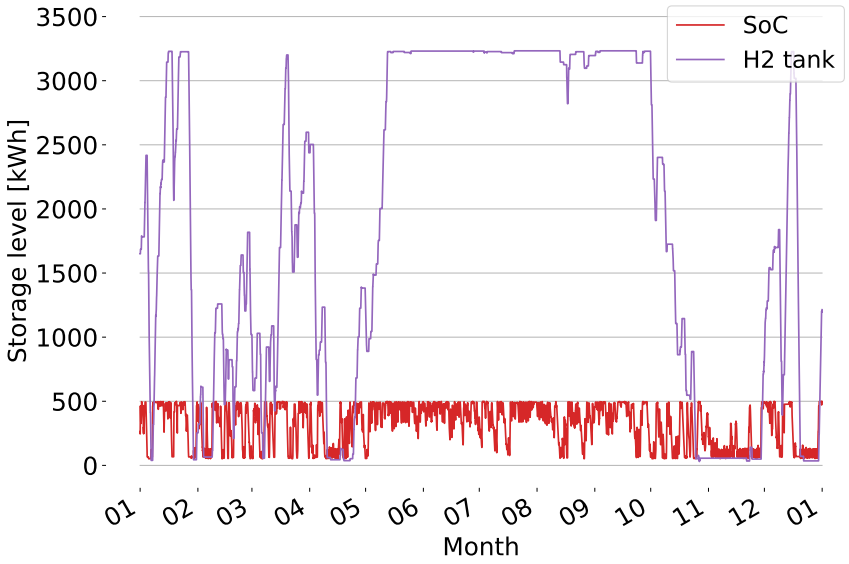

Figure 5.3: Energy level in the battery (SoC) and hydrogen tank (H2 tank) over the entire year for the base case simulation.

The hydrogen tank has large variations in its level over the course of the year. The speed at which it empties is rather high. In January the hydrogen tank has a sudden dip. From a completely full storage at the start of the 27th of January it empties in the afternoon of the 29th. All the available hydrogen was thereby used in less than three days.

The events in the end of January to the beginning of December are also noteworthy. Here, the energy levels go from completely empty, to full, and back to empty again. This happens within three weeks, and is mainly due to variations in wind generation.

5.2 Predictive control system

This section describes some of the intermediate results of creating the control system as well as its final implications on the operation. The intermediate results are the accuracy of the power predictions and the implications of objective function tweaking. The run time with different control horizons is also described.

5.2.1 Predictions

This section describes the accuracy of the prediction models created. Both the evaluation metrics and plots of the real and predicted powers are presented. The accuracy metrics caluclated are the normalized mean average error eq. (4.4), normalized root mean square error eq. (4.5) and coefficient of determination eq. (2.3).This is done for all three components: PV, Wind and Load.

PV

The description of how the solar prediction models were created may be found in section 4.2.1. During creation of the ML model, the coefficient of determination (R^2) was approximately 0.97. When tested on the simulation dataset, the accuracies achieved were as listed in table 5.1.

Table 5.1: Accuracy of PV prediction model when ran on simulation data (2019 and 2020). Normalized mean average error (nMAE), normalized root mean square error (nRMSE) and coefficient of determination (R^2).

Accuracy metric	Value
nMAE	0.0091
nRMSE	0.0254
R^2	0.9826

The real and predicted value of the PV powers for about 100 hours is plotted in fig. 5.4. It can be seen that the two follow each other very closely. Overall, the predicted value is rather close to the real output of the solar panels.

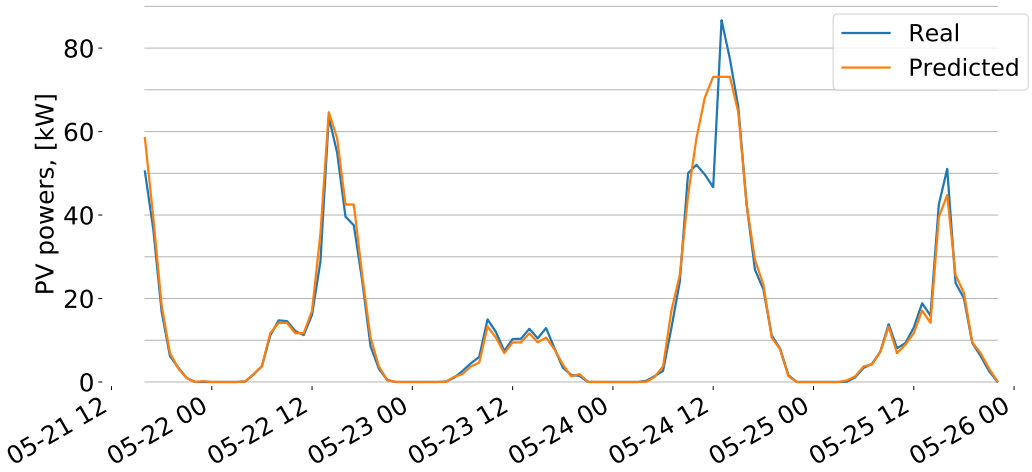

Figure 5.4: The predicted and real power of the PV-panels at Rye. The blue are the real measured values on site, and the orange are predicted by a machine learning algorithm.

Wind

The wind prediction models were created as described in section 4.2.1. When tested on the training dataset from sep-dec 2018 it reached an R^2 of 0.92. When it was ran on the simulation dataset (as described in section 4.4) it reached accuracies as in table 5.2.

Table 5.2: Accuracy of wind prediction model when ran on new data (2019 and 2020). Normalized mean average error (nMAE), normalized root mean square error (nRMSE) and coefficient of determination (R^2).

Accuracy metric	Value
nMAE	0.0534
nRMSE	0.0990
R^2	0.6944

For a visual representation of the predicted wind turbine powers, see fig. 5.5. As indicated by the accuracy it can be seen that this prediction model has larger deviations. It does however to a certain degree follow the actual output power of the turbine.

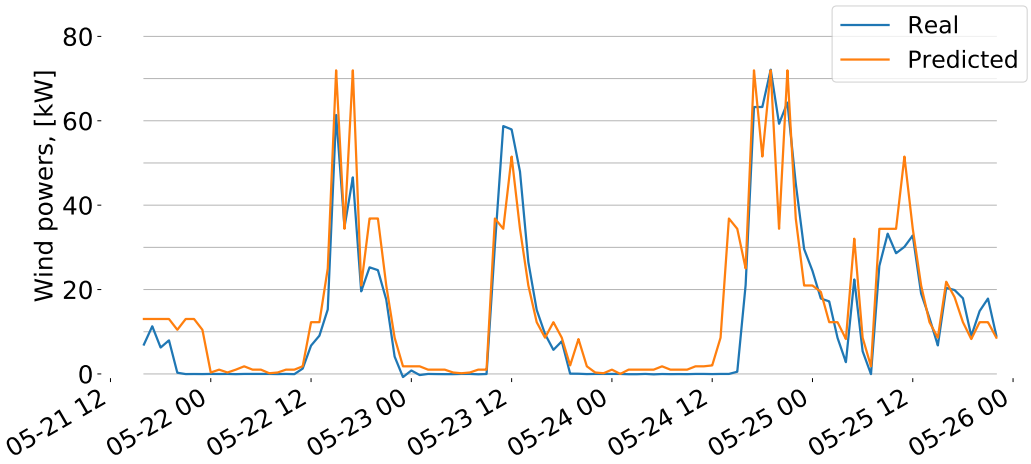

Figure 5.5: The predicted and real power of the wind turbine at Rye. The blue are the real measured values on site, and the orange are predicted by a machine learning algorithm.

Load

The load predictions were executed by a model created as described in section 4.2.1. When the first tests were ran during creation of the model, an R^2 of 0.53 was achieved. When the model thereafter was ran on the entire year of data for which the simulations are executed, the accuracies were as in table 5.3. The nominal power used for normalization was the maximum load measured.

Table 5.3: Accuracy of load prediction model when ran on new data (2019 and 2020). Normalized mean average error (nMAE), normalized root mean square error (nRMSE) and coefficient of determination (R^2).

Accuracy metric	Value
nMAE	0.0427
nRMSE	0.0688
R^2	0.5869

Some load predictions from May are shown in fig. 5.6. It is visible that there are plenty of deviations. The model has created a pattern that to a large degree repeats itself every day. The accuracy of these predictions could possibly be improved. The load is more unpredictable as it relates heavily on human behaviour, especially when analysing a single residential load. It was, however, attempted to include temperature measurements in the models. This made the predictions worse and the temperature was therefore excluded.

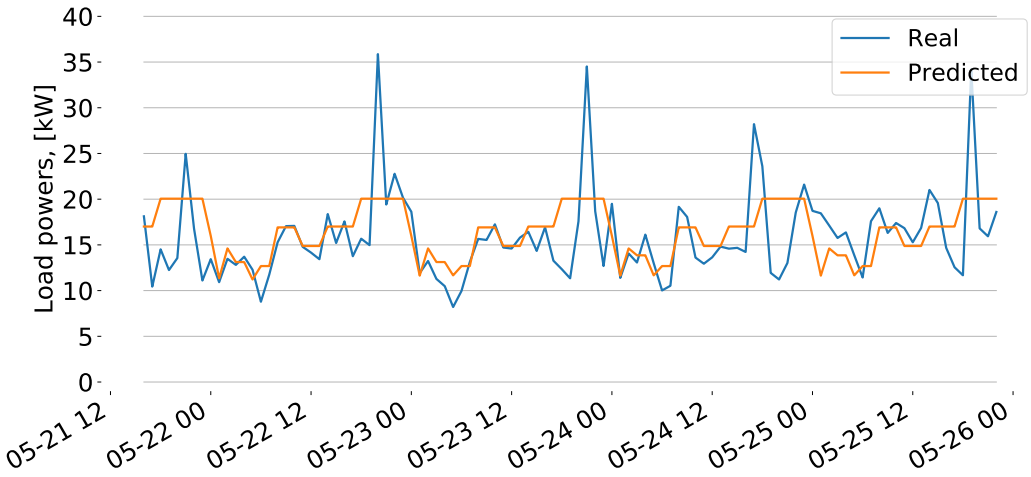

Figure 5.6: The predicted and real power of the load at Rye. The blue are the real measured values on site, and the orange are predicted by a machine learning algorithm.

5.2.2 Objective function

The objective function of the predictive control is described by eq. (4.12). It displays the objective function as a sum of five functions weighted in relation to each other. These weighing factors were tested with different values to evaluate their effect on the final performance. The full table of results is given in table 5.4. Because this analysis was conducted for 1500 simulation hours only, the coverage factors here are different than in the main results. A further analysis of the implications of altered weights could be executed, but due to long simulation time it was limited to these.

Table 5.4: Different objective function weights (eq. (4.12)) and their impact on central evaluation criteria. Tested for 1500 hours. Diesel coverage (eq. (5.2)), PV curtailment (eq. (5.5)), Wind curtailment (eq. (5.6)), Fuel cell coverage (eq. (5.4)), Battery coverage (eq. (5.3)).

Nr	a	b	c	d	e	Diesel	PV curtail	Wind curtail	Fuel cell	Battery
1	10	0	0.5	1	1	2.88%	7.84%	22.25%	15.84%	58.83%
2	10	0	0	1	1	3.87%	6.62%	18.64%	19.29%	59.58%
3	10	0.2	0.5	1.1	1	3.14%	3.33%	22.88%	16.03%	58.72%
4	10	0.2	0.5	1	1.2	3.00%	6.81%	19.04%	18.16%	57.61%
5	10	0	0.5	1	1.2	2.90%	6.78%	19.04%	17.86%	57.15%
6	**5**	**0.2**	**0.5**	**1**	**1.2**	**2.95%**	**6.54%**	**19.06%**	**18.08%**	**57.56%**
7	20	0.2	0.5	1	1.2	3.15%	6.70%	19.01%	18.18%	57.49%

As the top priority of the microgrid is to support the load with renewable power, limiting the diesel power is important. To ensure that this always triumphs, the weighting factor a is set to values far above the otherse. At all times where the management system finds a possibility of diesel generator usage within the control horizon, it must be prevented at all cost. The diesel generator power must therefore overshadow all other considerations, which is why its weighing factor is set several dimensions above the others.

The wind turbine is more difficult to curtail than the solar panels. This is because the wind turbine blades

must be mechanically braked. The d-factor, connected to the curtailed solar power is therefore set to 1, while the e-factor is set to 1.2 to limit the curtailment of wind power. These numbers are set relatively low compared to the diesel power as it is only to be considered during normal operation.

To limit excessive usage of storage components, the losses of the battery and hydrogen components are also considered. The factor related to the battery, b, is set to 0.2, while the hydrogen-factor, c, is set to 0.5. This is mainly to ensure that the battery deals with smaller variations in power. It is a faster component that is less degraded from power variations. As the hydrogen components are less suited for power variations and more vulnerable to degradation it is set higher. Compared to the other weighing factors however, they are low as it should not limit the system from using the battery and hydrogen when necessary. It can be seen from combination number 1 and 5 that setting b to zero gives a lower diesel consumption. Due to the significant component degradation of hydrogen units during over-usage, b is kept at 0.2.

Within the above discussed boundaries, the combinations 4, 6 and 7 are possible. Here, the factor a (diesel generator) is varied between 5, 10 and 20. The lowest resulting diesel usage was chosen, yielding an a of 5. In table 5.4 this combination is number 6, which will be the chosen objective function for all following simulation. It yielded the lowest dependency on the diesel generator and a reasonable operation of the other components.

5.2.3 Component utilisation

With accurate enough power predictions and an objective function that takes several considerations into account, the predictive control is in place. As a result, the microgrid is operating slightly differently. The state of the different components over the year are found in fig. 5.7. The battery is again operated very frequently. The electrolyser and fuel cell slightly less than the battery but significantly more than in the base case. The generator is operated in the same seasons, but seems to be used less.

The numerical quantification of how much power each component delivers are seen in eq. (5.7), eq. (5.9) and eq. (5.8). Both the battery and the fuel cell's contribution is increased considerably. The diesel generator's contribution is lowered from 13.45% in the base case to 6.90% with the predictive control.

$$\text{Diesel coverage} = \frac{E_{\text{Gen}}}{E_{\text{load}}} = \frac{12.15\text{MWh}}{176.18\text{MWh}} = 6.90\% \tag{5.7}$$

$$\text{Battery coverage} = \frac{E_{\text{batt, dch}}}{E_{\text{load}}} = \frac{113.48\text{MWh}}{176.18\text{MWh}} = 64.42\% \tag{5.8}$$

$$\text{Fuel cell coverage} = \frac{E_{\text{FC}}}{E_{\text{load}}} = \frac{31.12\text{MWh}}{176.18\text{MWh}} = 17.67\% \tag{5.9}$$

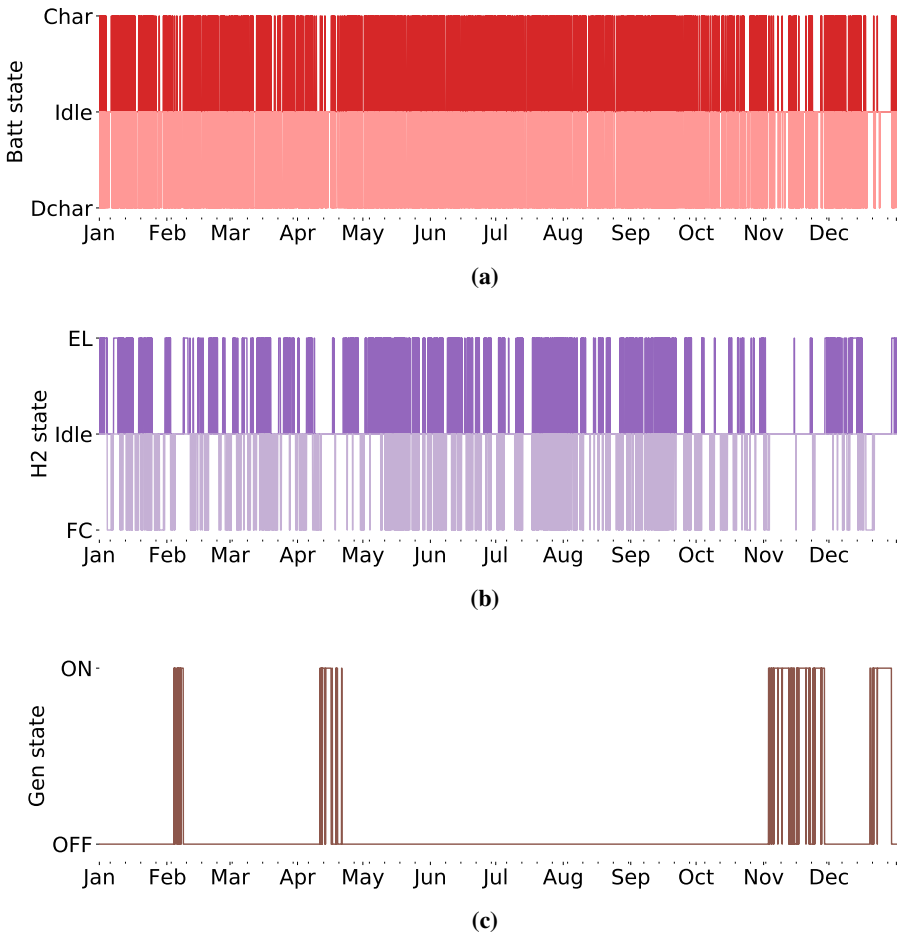

Figure 5.7: Predictive hourly states of the different components. (a) Battery states. Charging, discharging and idleness. (b) Hydrogen states. Electrolyser, fuel cell and idleness. (c) Generator states. ON and OFF.

The amount of available power generation that is curtailed is quantified by eq. (5.10) and eq. (5.11). Compared to the base case, both have gone down considerably.

$$\text{PV curtailment} = \frac{E_{\text{Curt, PV}}}{E_{\text{PV}}} = \frac{10.09\text{MWh}}{75.18\text{MWh}} = 13.34\% \tag{5.10}$$

$$\text{Wind curtailment} = \frac{E_{\text{Curt, Wi}}}{E_{\text{Wi}}} = \frac{26.26\text{MWh}}{190.56\text{MWh}} = 13.78\% \tag{5.11}$$

To visualize the energy situation in the grid, the storage levels of both the battery and hydrogen tank are shown in fig. 5.8. The overall situation is similar to the base case simulation. The input data and the components are the exact same. However, it is visually available that the hydrogen components are utilised more actively. This gives the high variations in storage level during the summer.

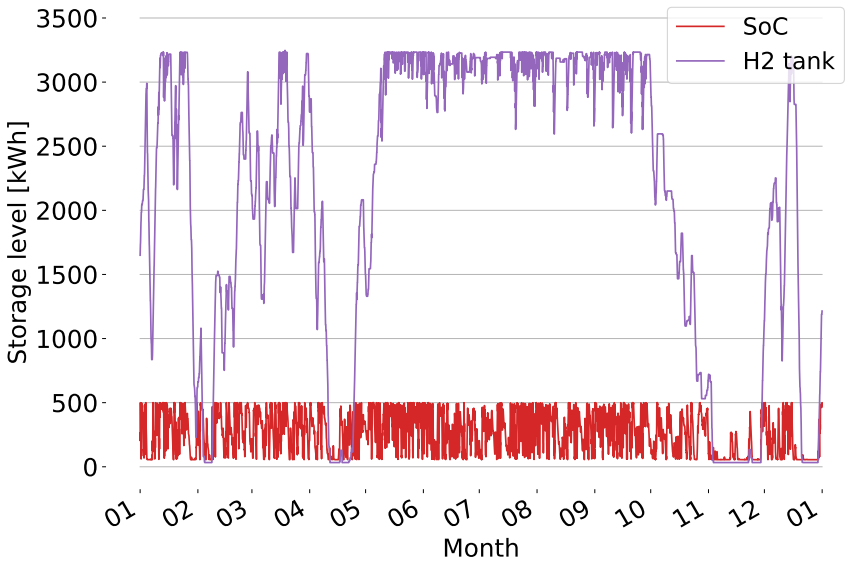

Figure 5.8: Energy level in the battery (SoC) and hydrogen tank (H2 tank) over the entire year. From the predictive simulation.

5.2.4 Run time

As the implemented control system would has to be run every hour in a live system its run time is an important parameter. As an actual live system would need data fetching from external sources as well as an extra buffer, the simulation in this modelling should take up limited amounts of this hour. A test was run to check its average time use per hour. The modelling was done on a MacBook Air from 2014 with operating system Catalina (10.15.4), a 1.4 GHz Dual-Core Intel Core i5 Processor and a 4 GB 1600 MHz DDR3 memory.

The test was executed on 1500 hours with different control horizons: 24 and 48 hours. For every hour in the control horizon, the optimisation algorithm complexity increases significantly. Variables for all powers and levels as well as all constraints must be created for every time step in the optimisation. During the test with a 24 hour control horizon, the average time for one hour was 0.42 seconds. The longest time spent on one hour was 16.6 seconds. This suggests no issue with run time thus far. During the test with a control horizon of 48 hours, the average time was 1.42 seconds per hour. This equals a 238% rise in the average time. The hour with the longest run time elapsed for 179.8 seconds or 3 minutes, which is more than 10 times that of the previous test. In addition, the number of infeasible optimisations also increased. This showcases the run time's vulnerability to the control horizon parameter. With a time window of 60 minutes between each iteration this should still not be problematic. There are still large safety margins and the run time could also be reduced by more computational power and restructure of the code.

5.3 Comparison of behaviour

This sections aims to better describe how the two control systems differ. It was found in the previous section that there is a large differences on the overall numbers. This section aims to compare this differences in further deatil. A summary of the energy supplied by each component is given. In addition some shorter time periods are chosen to exemplify what this means on the daily and hourly level.

Energy output per component

As seen by the previously presented numbers and plots, the control system is important for the grid operation. There is a significant difference in how much energy each component supplies to the microgrid. A comparison between the energy supplied by each component in the two operational methods is given in table 5.5. The results are given as the absolute, numerical values and the percentwise change of the predictive control compared to the base case.

Table 5.5: Comparison between the two systems: base case and predictive control system. Absolute values of the amount of energy the component supplies over the entire year.

Component	Base case [MWh]	Predictive [MWh]	Percentwise change
Diesel	23.69	12.15	- 48.71 %
Battery	54.08	113.48	+ 109.84%
Fuel cell	12.76	31.12	+ 143.89 %
Electrolyser	44.86	102.48	+ 128.44 %
PV curtailment	18.55	10.09	- 45.61%
Wind curtailment	85.43	26.26	- 69.26%

1: Preventing storage running empty

The first interesting timing that shows a different operation between the two systems are six days in early January, displayed in fig. 5.9. Here, the base case storage units run empty and the generator has to be started. The predictive control however manages to keep the storage levels higher, and the diesel generator is prevented from starting.

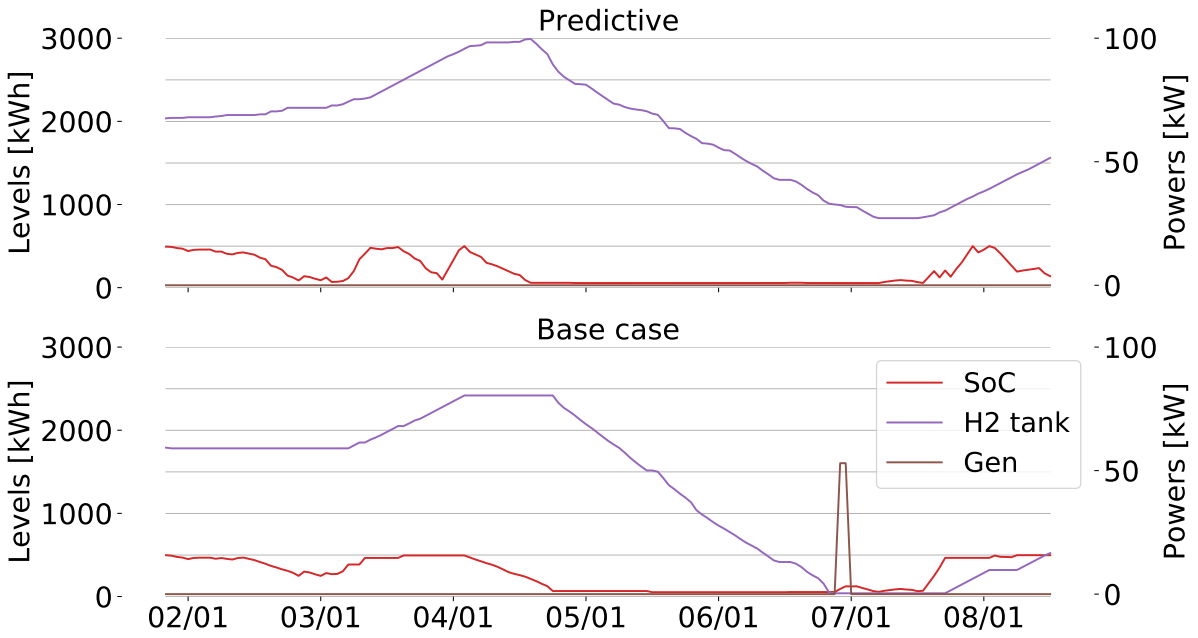

Figure 5.9: Comparison between the two designed control systems (Base case and Predictive). It shows how the battery (SoC) and hydrogen (H2 tank) run empty i the base case, leading to the diesel generator (Gen) being used. In the predictive control this is prevented.

2: Limit generator usage once storage is empty

The second interesting timing is two weeks in mid April, displayed in fig. 5.10. Here, both storage units in both cases run empty. The way the backup diesel generator is used to compensate for it varies between the two cases. In the base case, the generator is run at maximum power to recharge the battery. The leads to the generator being used a lot. Over the whole plotting period, the diesel generator supplies 2915 kWh. In the predictive case however, the diesel generator power varies according to the load. In this case, the diesel generator supplies 1205 kWh, ie. 58.7% less than in the base case.

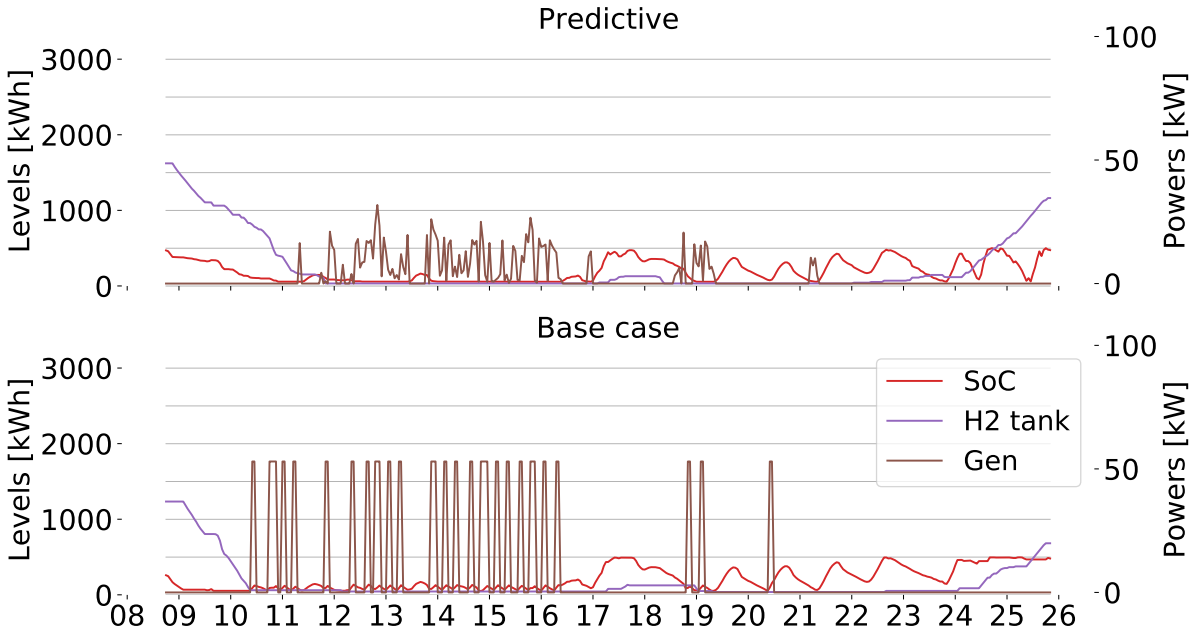

Figure 5.10: Comparison between the two designed control systems (Base case and Predictive) for two weeks in April. It shows how the battery (SoC) and hydrogen (H2 tank) run empty in both cases. The usage of the diesel generator (Gen) varies significantly between the two. In the base case, the generator is always operated at maximum power. In the predictive, the diesel power usage varies with the load.

3: Over-usage of storage units

In a third example the situation is monitored when there is excess energy in the system. Five days in August are pictured to show how the control systems behave differently. The predictive control has a larger variation in battery SoC. It seems to plan such that the SoC barely reaches its maximum when the production units stop producing. This makes a storage profile in both units with variations that seem unnecessary large. This type of operation may damage the components and should be avoided. The base case has smoother energy levels, which will cause the components less harm and still supply the load.

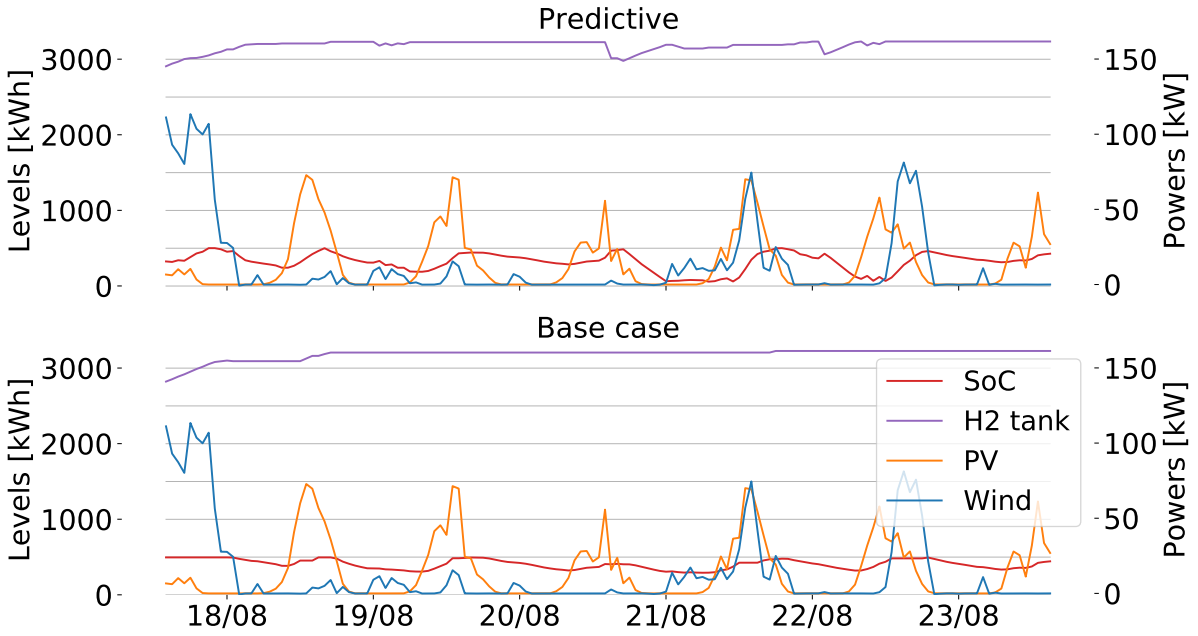

Figure 5.11: Comparison between the two designed control systems (Base case and Predictive) for two weeks in April. It shows how the battery (SoC) and hydrogen (H2 tank) are rather full. The variation in solar power (PV) and wind power (Wind) is also shown. The predictive control seems to have unnecessary large variation in both the battery and the hydrogen level.

Chapter 6 Discussion and Future Work

The microgrid operation has successfully been modelled in two ways. Its results lead to several insights on both the general function of the system as well as on the different control systems. This chapter aims to discuss the results and their implication, as well as weaknesses in the modelling.

6.1 Evaluation of operation

Using measurements of the already installed components and technical information on the remainder of the components, the operation over one year yields several insights. It is found that the goal of limiting the use of the diesel generator to 5% is challenging in terms of energy delivered. In the base case, 13.45% (23.69 MWh) of the load energy come from the diesel generator. In the predictive solution, the same number amounts to 6.90% (12.15 MWh). The diesel usage has gone down significantly, with the energy generation from diesel being reduced with 48.71%. This suggests a significant improvement with the newly designed operation. However, it still results in too much energy being supplied by the fossil fuelled generator.

But, there is another way to analyse the numbers. The utilisation factor of a component is given by the number of active hours divided by the number of total hours. When this is calculated for both the base case and the predictive control, the diesel generator has a utilisation factor of 5.09% and 9.97% respectively. When looking at these numbers the goal of 5% is further within reach, and it also alters the view on which control system delivers the best result. Still, the amount of emissions from the diesel is more tightly related to the energy it generates than to the number of hours it is active. The coverage factor is therefore chosen as the metric to evaluate the system, and not the utilization factor.

As designed, the battery is responsible for the smaller variations and the hydrogen for the seasonal changes in available energy. The two storage units in this manner seem to compliment each other. The simulations show a certain vulnerability to longer periods without power generation. There are examples of the hydrogen tank running empty in less than three days, which is less than expected for a unit with seasonal ambitions.

With the large amount of energy supplied by the diesel generator in mind, the amount of energy curtailed is high. In the base case, the PV curtailment and wind curtailment was as high as 24.67% and 44.83% respectively. This showcases the importance of the timing of power generation and the necessity of large storage units.

When the system was designed, it was for an annual load of 126.75 MWh. With the load for the simulated year reaching 176.18 MWh, the increase of load for the microgrid to supply was 39%. This is substantial and may be due to natural yearly variations as well as a known increase in demand on the farm. Supplying a single residential farm load is challenging as it volatile and vulnerable to changes from new equipment and other social factors. This may be a root cause for the struggles to limit the generator usage.

The predictive control system as implemented for this thesis may be more challenging for component health. As seen in fig. 5.11, both the battery and the hydrogen components are used very actively. For such chemical components, this may lead to unnecessary stress and thereby component degradation. This could probably be better accounted for by altering the objective function.

It may also be important to note that if all the coverage factors of the predictive control are added, they will account to more than 100%. The coverage factors are a percentage of the component's delivered energy, in relation to the load. When summarizing the coverage factors of the diesel, battery, fuel cell, PV and wind this will exceed 100% as they supply power to each other as well as to the load.

6.2 Modelling shortcomings and strengths

When executing a modelling such as the two executed for this thesis there are always shortcomings. These shortcomings, as well as different strengths of each system is discussed in this section.

General for both control systems

One of the larger pieces of the puzzle that still remains is to ensure that this management system incorporates well with local controllers. The simulation executed has a temporal resolution of one hour, while the control of the microgrid has to happen in real time. It must therefore be ensured that the management implemented combines well with the local controllers of each individual component in the microgrid. Researching this field may bring changes to the control system and make it more trustworthy.

As mentioned in Chapter 3, the hydrogen components (electrolyser and fuel cell) have dynamic efficiencies. The efficiency varies with the amount of input power to (electrolyser) or output power (fuel cell) from the component. In the simulation this was simplified into an average efficiency. This should be taken into consideration by making functions for their varying efficiency. As none of the simulations have it implemented, the comparison between the two should not be much distorted. It would be interesting to see what role it could play when implemented.

When building a historical simulation, faulty measurements are always an issue. As discussed in section 4.4, the data used is gathered from different measuring devices with different limitations. Faults might occur during the measuring, when sending the data and during storing of the gathered data points. As the whole simulation builds upon these values, faults may have implications for the result.

This simulation is executed without including considerations of maintenance and other outages. As the system holds many technically complicated components that have not been put in play in the same manner, faults might occur. Such faults or general maintenance may influence the operation in ways not taken into consideration.

Base case

The base case simulation is based upon a few technical descriptions and an interview with Powidian. As the model was created with limited collaboration with those implementing the control system, there may have been misunderstandings. The management system of the base case is implemented to the best of the authors ability but could have faults due to outdated information, insufficient interviews or changed strategies.

One feature that is implemented in the real microgrid, that was not taken into account in the simulation, is the details around the fuel cell logic. The controller on site is focused on keeping the fuel cell power

in a certain range to stay within its maximum operating point as shown in fig. 3.7. This has not been considered in this implementation as the efficiency is averaged. Some details in the dynamic functionality of the fuel cell might therefore be lost.

One of the most clear advantages of the base case implementation is its limited computational effort. This both limits the design complexity during the creation of the logic as well as during operation. Powidian has a long experience in these control systems which is beneficial when using a control system in a new grid. Introducing a new control system design might give rise to operational challenges that could cause extra downtime. As electricity is a vital commodity this is important to limit.

Predictive control

The first steps of the predictive control system are the power predictions. The most pressing problem on these predictions are the training data availability. The wind power model was built on data from three months in 2018. The other two models had to be built on some of the same data as those used in the simulation. This is not possible when creating the control system for a new microgrid. The PV and load predictions may therefore be more accurate than what is likely in the real world. But, there are many ways to improve predictions that have not been researched thoroughly enough. These considerations may therefore balance eachother out to a certain extent. The predictions can be implemented recursively, ensuring that the models are continuously improved with new data points.

Another important matter on the predictions is finishing the pipeline. The models built in this thesis rely on historical measurements on site. When setting a system like this live, the input parameters must be weather predictions as illustrated by fig. 2.2. Another important research area is therefore which data sources are available for weather forecasts and their implications for the prediction accuracy.

One important feature of the predictive management system implemented, is how easily the behaviour can be altered by changing the objective function. As briefly discussed in section 5.2.2, the weighting factors can easily be adjusted. These have a large effect on how the power is distributed among the components. The variations in this research was limited by the time, and should be further optimised. Weighting factors can be altered to change priorities and new components added to the objective function to further improve the operation. This gives a large flexibility in altering the behaviour of the operation, without changing much in the logic. That represents an advantage of such a system.

One important trade-off when designing a system as the predictive control described here, is the computational effort versus the control horizon. As briefly discussed in section 5.2.4, the average run time per hour increased by 238% when changing the control horizon from 24 to 48 hours. The maximum run time per hour also increased by more than 10 times. The computational complexity must therefore be monitored closely when implementing new features. Limitations on the time spent at each optimisation can also be set. If the optimisation in one time step exceeds a certain threshold an error can be thrown, causing the backup solution (as described in section 4.3.3) to be triggered. The weather forecasts quality and thereby the prediction accuracies also vary greatly when predicting powers far in the future. This decreases the potential gain of having a larger control horizon.

Another trade-off to consider when designing such a system is between limiting the optimisation's freedom and limiting undesired behaviour. On one hand, the undesired behaviour of the predictive control can often be limited by imposing new constraints in the optimisation or new evaluations for the objective function. This gives an operation that is more likely to fall within the desired frames. On the other hand, it also limits the optimisation's freedom to find the best operation. It might therefore give a less optimal solution and work against the concept of letting the algorithm decide the best power sharing logic. These considerations must be evaluated at every new addition to the optimisation problem.

The design of a management system is different to implement on-site, with control signals being sent to the physical components, than simply a simulation on one computer. Therefore, modularity is important during implementation. If this method is to be implemented by another developer it is important that the operation is broken down into smaller functions with a limited scope and responsibility. The separate functions must be replaceable by other techniques or technologies without too much alteration. For example, the data fetching methodology is likely to be very different in different implementations. This has been the focus throughout the code and should make it easier to use in different systems.

6.3 General learning outcomes

When designing a microgrid in the start phase of the project, it may seem as though the component choice and sizing are the only determining factors. This thesis proves that the operational strategy also massively alters the results. The hunt for the perfect control system might not be finalised, but its importance is a fact.

Another important task highlighted by implementing this control system is measuring. In a world where data driven methodologies become more prominent, the existence of good measurement systems is more important. In order to utilise methodologies such as machine learning, a large foundation of data must be available. There must therefore be enough measurements of important parameters. The measurements must be of a fine enough time resolution and stored for a sufficiently long period. All data contain interruptions, faults and inaccuracies, but decreasing these highly improve their value.

6.4 Future work

The designed control system is open for several improvements. First, the dynamic efficiencies of the electrolyser and fuel cell should be implemented. In these simulations they were averaged, but in reality they vary with the components power, as previously described. Second, the objective function can be improved. This includes incorporating new considerations (such as component degradation) as well as further optimising the weighting factors. A cost based optimisation could also be a way forward.

To make the simulation closer to reality, the prediction pipeline must be completed. The machine learning models must be built on weather forecasts and not measured historical data. Forecasts of weather must be translated into input parameters such as irradiance and wind speed. In this way the true accuracy of power predictions can be found. There are also more advanced machine learning techniques to be explored, in order to make the most accurate models.

As briefly discussed in section 2.1, the energy management system is not the entire control system. If a hierarchical control architecture is chosen, it must be researched how this operational strategy ban be implemented with the local controllers. Further research on how the set points found (secondary control) are implemented in the local controllers (primary control) could be interesting. These interactions could unveil important new aspects to consider, both opportunities and constraints.

Other scheduling models could also be implemented. Short-term and long-term scheduling may be combined, with the goal of more effectively utilising both energy storage systems.

It was unclear how machine learning power predictions could benefit the system when this project was initiated. Other areas of applications of machine learning could therefore be important to research. Fault detection might be one such area. Many components are present in the microgrid and to monitor their behaviour would possibly bring new insights and prevent outages and expensive maintenance. This has been an area of great research in the latest years[56, 57, 58]. Other possibilities of the application

of machine learning could be load scheduling[59], stability analysis of both grid connected and island operated microgrids [58, 60] and state of charge estimations for battery[61, 62]. [63]

Chapter 7 Conclusion

This thesis has analysed the management of an island operated microgrid. Two different operational strategies have been implemented: a rule based system (base case) and a predictive control. The simulations have been executed on a real microgrid being developed by TrønderEnergi through the EU-funded project REMOTE.

Measurements for a year of generation and load were utilised to simulate the component behaviour. The generation from the photovoltaic solar panels and wind turbine was as expected during the design phase of the microgrid. The load however, increased by 39%. A goal of the microgrid operation is to have 95% of the energy come from renewable sources. In the base case, the diesel generator supplied 54.08 MWh, which equates to 13.45% of the load.

The predictive control designed utilises machine learning models to predict PV and wind generation as well as load consumption. The generating unit predictions (PV and wind) achieved higher accuracy than those of the load. These power predictions are input to a control algorithm, that in every time step equates the optimal power from each component. This is done by a optimisation algorithm over a certain control horizon. The influence of changing the objective function of this optimisation is evaluated. Evaluating one year of operation, the energy from the diesel generator is now 12.15 MWh. This makes up 6.90% of the load and means a decrease of 48.71% compared to the base case.

Some comparison of the behaviour of the two different management systems are conducted. In certain periods, the predictive control prevents the generator from having to be activated. When the generator is activated in both cases, the base case operates the diesel generator at full power until the battery has reached a satisfactory level. The predictive control operates the generator such that it only just covers the load. To improve the management system, it should be researched how the damage to the involved components can be reduced. An effort to complete the prediction pipeline should also be made.

The management system was implemented in Python, using the optimisation tool Pyomo. The architectural details of the project have been described and should make it easier to use at Rye or other microgrids.

The large difference in operation between the two implemented solutions show the importance of a good control system. It can alter how independently an islanded microgrid can function, and thereby the success of the project. The recent improvements in computational power and data analysis matureness enables this control system. The accurate predictions of intermittent generating units and load in combination with optimisation are at the core of the predictive control system. As it was found that the diesel consumption was reduced significantly, this case study shows the potential of this state-of-the art solution. Hopefully, it will contribute to more remote and renewable energy supplies being successful.

Bibliography

[1] D. E. Olivares, A. Mehrizi-Sani, A. H. Etemadi, C. A. Cañizares, R. Iravani, M. Kazerani, A. H. Hajimiragha, O. Gomis-Bellmunt, M. Saeedifard, R. Palma-Behnke, G. A. Jiménez-Estévez, and N. D. Hatziargyriou. Trends in microgrid control. *IEEE Transactions on Smart Grid*, 5(4):1905–1919, 2014.

[2] S. Theocharides, G. Makrides, G. E. Georghiou, and A. Kyprianou. Machine learning algorithms for photovoltaic system power output prediction. In *2018 IEEE International Energy Conference (ENERGYCON)*, pages 1–6, June 2018.

[3] Katherine Woodruff. Introduction to boosted decision trees. `https://indico.fnal.gov/event/15356/contribution/1/material/slides/0.pdf`, 2017. NM State University. Accessed: November 2019.

[4] Maylis Duru and Trond Rikard Olsen. Site specifications v2.3. Unpublished, May 2018.

[5] Marta Gandiglio Massimo Santarelli (POLITO) Paolo Marocco, Domenico Ferrero. Remote – deliverable d2.2: Technical specification of the technological demonstrators. `https://www.remote-euproject.eu/deliverables/`, jul 2018.

[6] NVE. Vindkraftdata, produksjonsdata. `https://www.nve.no/energiforsyning/vindkraft/vindkraftdata`, 2019. Accessed: 17th March 2020.

[7] SolarEdge. Microgrid Rye Summary Report. Unpublished, October 2018.

[8] PowiDian. Technical offer - energy storage solution. Technical Proposal ESS Vers: 1, Unpublished, oct 2018.

[9] Delphine Wagner, Bernhard Kvaal, Villy Biltoft, and Stefan Knauf. Remote area energy supply with multiple options for integrated hydrigen-based technologies - deliverable number 4.3. Confidential, June 2019.

[10] VESTAS. *General Specification VESTAS V27-225kW, 50 Hz Windturbine with tubular/lattice tower*. `http://www.husdesign.no/lars/V27-Teknisk%20spesifikasjon/gen%20specification%20v27.pdf`, January 1994.

[11] Campsim. Steady state study report - remote project. Unpublished, April 2019.

[12] Solbes. Systeminformasjon materiell. Unpublished, 2018.

[13] Kohler SDMO. J66k. Technical report, SDMO, Kohler, September 2018. Technical specification of generator.

[14] NVE. Leveringsplikt. `https://www.nve.no/reguleringsmyndigheten/nettjenester/nettilknytning/leveringsplikt/`, 2019. Accessed: 10th December 2019.

[15] Anniken Auke Borgen (TrønderEnergi). Personal communication, autumn 2019.

[16] S. Aslam, H. Herodotou, N. Ayub, and S. M. Mohsin. Deep learning based techniques to enhance the performance of microgrids: A review. In *2019 International Conference on Frontiers of Information Technology (FIT)*, pages 116–1165, 2019.

[17] S. F. Rafique and Z. Jianhua. Energy management system, generation and demand predictors: a review. *IET Generation, Transmission Distribution*, 12(3):519–530, 2018.

[18] Nina Lindholm. Prediction models of solar- and wind power gen-eration by machine learning in rye microgrid. Master's thesis, Norwegian University of Scienece and Technologies (NTNU), 2019. Unpublished.

[19] X. Zhou, T. Guo, and Y. Ma. An overview on microgrid technology. In *2015 IEEE International Conference on Mechatronics and Automation (ICMA)*, pages 76–81, Aug 2015.

[20] B. Kroposki, T. Basso, and R. DeBlasio. Microgrid standards and technologies. In *2008 IEEE Power and Energy Society General Meeting - Conversion and Delivery of Electrical Energy in the 21st Century*, pages 1–4, July 2008.

[21] S. Jadidi, H. Badihi, and Y. Zhang. A review on operation, control and protection of smart microgrids. In *2019 IEEE 2nd International Conference on Renewable Energy and Power Engineering (REPE)*, pages 100–104, 2019.

[22] S. A. Chandler, J. H. Rinaldi, R. B. Bass, and L. Beckett. Smart grid dispatch optimization control techniques for transactive energy systems. In *2014 IEEE Conference on Technologies for Sustainability (SusTech)*, pages 51–54, 2014.

[23] N. Telu, R. G. Rao, and V. S. Vakula. Optimal planning and operation of microgrid: A comprehensive review. In *2018 International Conference on Recent Innovations in Electrical, Electronics Communication Engineering (ICRIEECE)*, pages 1167–1174, 2018.

[24] T. V. Vu, S. Paran, F. Diaz, T. El Meyzani, and C. S. Edrington. Model predictive control for power control in islanded DC microgrids. *IECON 2015 - 41st Annual Conference of the IEEE Industrial Electronics Society*, pages 1610–1615, 2015.

[25] Mohammad B. Shadmand, Robert S. Balog, and Haitham Abu-Rub. Model predictive control of PV sources in a smart DC distribution system: Maximum power point tracking and droop control. *IEEE Transactions on Energy Conversion*, 29(4):913–921, 2014.

[26] David Morin, Yoann Stevenin, Cédric Grolleau, and Pascal Brault. Evaluation of performance improvement by model predictive control in a renewable energy system with hydrogen storage. *International Journal of Hydrogen Energy*, 43(45):21017–21029, 2018.

[27] J. Ma and X. Ma. State-of-the-art forecasting algorithms for microgrids. In *2017 23rd International Conference on Automation and Computing (ICAC)*, pages 1–6, 2017.

[28] Antonio Criminisi, Jamie Shotton, and Ender Konukoglu. *Decision Forests: A Unified Framework for Classification, Regression, Density Estimation, Manifold Learning and Semi-Supervised Learning*, volume 7. NOW Publishers, foundations and trends® in computer graphics and vision: vol. 7: no 2-3, pp 81-227 edition, January 2012.

[29] SciKit Learn - Regression Metrics. `https://scikit-learn.org/stable/modules/model_evaluation.html#regression-metrics`. Accessed: 2020-05-15.

[30] Gilbert M. Masters. *Renewable and Efficient Electric Power Systems*. John Wiley & Sons, 2 edition, 2013.

[31] REC. *REC TwinPeak 2 Series - Datasheet*. https://www.recgroup.com/sites/default/files/documents/ds_rec_twinpeak_2_series_iec_rev_i_en_web.pdf.

[32] A. Almadhor. Performance prediction of distributed pv generation systems using artificial neural networks (ann) and mesh networks. In *2018 International Conference on Smart Grid (icSmartGrid)*, pages 88–91, Dec 2018.

[33] K. Benhmed, F. Touati, M. Al-Hitmi, N. A. Chowdhury, A. S. P. Gonzales, Y. Qiblawey, and M. Benammar. Pv power prediction in qatar based on machine learning approach. In *2018 6th International Renewable and Sustainable Energy Conference (IRSEC)*, pages 1–4, Dec 2018.

[34] S. Theocharides, V. Venizelou, G. Makrides, and G. E. Georghiou. Day-ahead forecasting of solar power output from photovoltaic systems utilising gradient boosting machines. In *2018 IEEE 7th World Conference on Photovoltaic Energy Conversion (WCPEC) (A Joint Conference of 45th IEEE PVSC, 28th PVSEC 34th EU PVSEC)*, pages 2371–2375, June 2018.

[35] D. Su, E. Batzelis, and B. Pal. Machine learning algorithms in forecasting of photovoltaic power generation. In *2019 International Conference on Smart Energy Systems and Technologies (SEST)*, pages 1–6, Sep. 2019.

[36] Qu Xiaoyun, Kang Xiaoning, Zhang Chao, Jiang Shuai, and Ma Xiuda. Short-term prediction of wind power based on deep long short-term memory. In *2016 IEEE PES Asia-Pacific Power and Energy Engineering Conference (APPEEC)*, pages 1148–1152, Oct 2016.

[37] R. Ak, O. Fink, and E. Zio. Two machine learning approaches for short-term wind speed time-series prediction. *IEEE Transactions on Neural Networks and Learning Systems*, 27(8):1734–1747, Aug 2016.

[38] L. Guo, C. Wang, P. Gao, Y. Wang, Y. Zhong, and M. Huang. An online short-term wind power prediction considering wind speed correction and error interval evaluation. In *2014 International Conference on Information Science, Electronics and Electrical Engineering*, volume 1, pages 28–32, April 2014.

[39] M. Barque, S. Martin, J. E. N. Vianin, D. Genoud, and D. Wannier. Improving wind power prediction with retraining machine learning algorithms. In *2018 International Workshop on Big Data and Information Security (IWBIS)*, pages 43–48, May 2018.

[40] S. Netsanet, J. Zhang, D. Zheng, R. K. Agrawal, and F. Muchahary. An aggregative machine learning approach for output power prediction of wind turbines. In *2018 IEEE Texas Power and Energy Conference (TPEC)*, pages 1–6, Feb 2018.

[41] Xiaoxia Zheng. Electric load forecasting using Bayesian least squares support vector machine. *Proceedings - 2010 6th International Conference on Natural Computation, ICNC 2010*, 2(Icnc):880–883, 2010.

[42] Liu Limei and Hou Xuan. Study of electricity load forecasting based on multiple kernels learning and weighted support vector regression machine. *Proceedings of the 29th Chinese Control and Decision Conference, CCDC 2017*, pages 1421–1424, 2017.

[43] Philipp Theile, Anna Linnea Towle, Kaustubh Karnataki, Alessandro Crosara, Kaveh Paridari, Graham Turk, and Lars Nordstrom. Day-ahead electricity consumption prediction of a population of households: Analyzing different machine learning techniques based on real data from RTE in France. *2018 IEEE International Conference on Communications, Control, and Computing Technologies for Smart Grids, SmartGridComm 2018*, pages 1–6, 2018.

[44] Jingjie Yang and Qiang Wang. A Deep Learning Load Forcasting Method Based on Load Type Rcognition. *Proceedings - International Conference on Machine Learning and Cybernetics*, 1:173–177, 2018.

[45] Roya Ahmadiahangar, Tobias Häring, Argo Rosin, Tarmo Korõtko, and João Martins. Residential Load Forecasting for Flexibility Prediction Using Machine Learning-Based Regression Model. *Proceedings - 2019 IEEE International Conference on Environment and Electrical Engineering and 2019 IEEE Industrial and Commercial Power Systems Europe, EEEIC/I and CPS Europe 2019*, pages 6–9, 2019.

[46] H. Mori and E. Kurata. An efficient kernel machine technique for short-term load forecasting under smart grid environment. *IEEE Power and Energy Society General Meeting*, pages 1–4, 2012.

[47] Remote website. `https://www.remote-euproject.eu`. Accessed: May 2020.

[48] Solbes. Pvsyst simulation energy report. Unpublished, February 2019.

[49] Powidian Delphine Wagner. Personal communication, 2019.

[50] Claude Lamy. From hydrogen production by water electrolysis to its utilication in a pem fuel cell or ina so fuel cell: Some considerations on the energy efficiencies. *International Journal of Hydrogen Energy*, 41(34):15415–15425, September 2016.

[51] F. Pedregosa, G. Varoquaux, A. Gramfort, V. Michel, B. Thirion, O. Grisel, M. Blondel, P. Prettenhofer, R. Weiss, V. Dubourg, J. Vanderplas, A. Passos, D. Cournapeau, M. Brucher, M. Perrot, and E. Duchesnay. Scikit-learn: Machine learning in Python. *Journal of Machine Learning Research*, 12:2825–2830, 2011.

[52] William E Hart, Jean-Paul Watson, and David L Woodruff. Pyomo: modeling and solving mathematical programs in python. *Mathematical Programming Computation*, 3(3):219–260, 2011.

[53] William E. Hart, Carl D. Laird, Jean-Paul Watson, David L. Woodruff, Gabriel A. Hackebeil, Bethany L. Nicholson, and John D. Siirola. *Pyomo–optimization modeling in python*, volume 67. Springer Science & Business Media, second edition, 2017.

[54] LLC Gurobi Optimization. Gurobi optimizer reference manual. `http://www.gurobi.com`, 2020.

[55] Stefan Pfenninger and Iain Staffell. Long-term patterns of European PV output using 30 years of validated hourly reanalysis and satellite data. *Energy*, 114:1251–1265, 2016.

[56] Anusuya Arunan, Jayashri Ravishankar, and Eliathamby Ambikairajah. Centralized voltage signal-based fault detection and classification for islanded ac microgrid. 04 2020.

[57] M. Mishra and P. K. Rout. Detection and classification of micro-grid faults based on hht and machine learning techniques. *IET Generation, Transmission Distribution*, 12(2):388–397, 2018.

[58] M. Al Karim, J. Currie, and T. Lie. Dynamic event detection using a distributed feature selection based machine learning approach in a self-healing microgrid. *IEEE Transactions on Power Systems*, 33(5):4706–4718, 2018.

[59] M. Sung and Y. Ko. Machine-learning-integrated load scheduling for reduced peak power demand. *IEEE Transactions on Consumer Electronics*, 61(2):167–174, 2015.

[60] C. Lassetter, E. Cotilla-Sanchez, and J. Kim. A learning scheme for microgrid reconnection. *IEEE Transactions on Power Systems*, 33(1):691–700, 2018.

[61] M. S. Sidhu, D. Ronanki, and S. Williamson. State of charge estimation of lithium-ion batteries using hybrid machine learning technique. In *IECON 2019 - 45th Annual Conference of the IEEE Industrial Electronics Society*, volume 1, pages 2732–2737, 2019.

[62] X. Hu, S. E. Li, and Y. Yang. Advanced machine learning approach for lithium-ion battery state estimation in electric vehicles. *IEEE Transactions on Transportation Electrification*, 2(2):140–149, 2016.

[63] S. M. Miraftabzadeh, F. Foiadelli, M. Longo, and M. Pasetti. A survey of machine learning applications for power system analytics. In *2019 IEEE International Conference on Environment and Electrical Engineering and 2019 IEEE Industrial and Commercial Power Systems Europe (EEEIC / I CPS Europe)*, pages 1–5, 2019.

[64] Pandas - Python Data Analysis Library. `https://pandas.pydata.org/`. Accessed: 2020-03-05.

Appendix

Basecase: Data structures

The base case control system is implemented in python. One data structure dominates the code: the Pandas DataFrame. These are a high level data structure based on numpy arrays, especially designed for data analysis.[64] There are three DataFrames created in the code: P_{in}, P_{calc} and Levels. These have 5, 8 and 3 columns respectively, as pictured in fig. 7.1. The Dataframes are as long as the simulation horizon ($\sim$8760h).

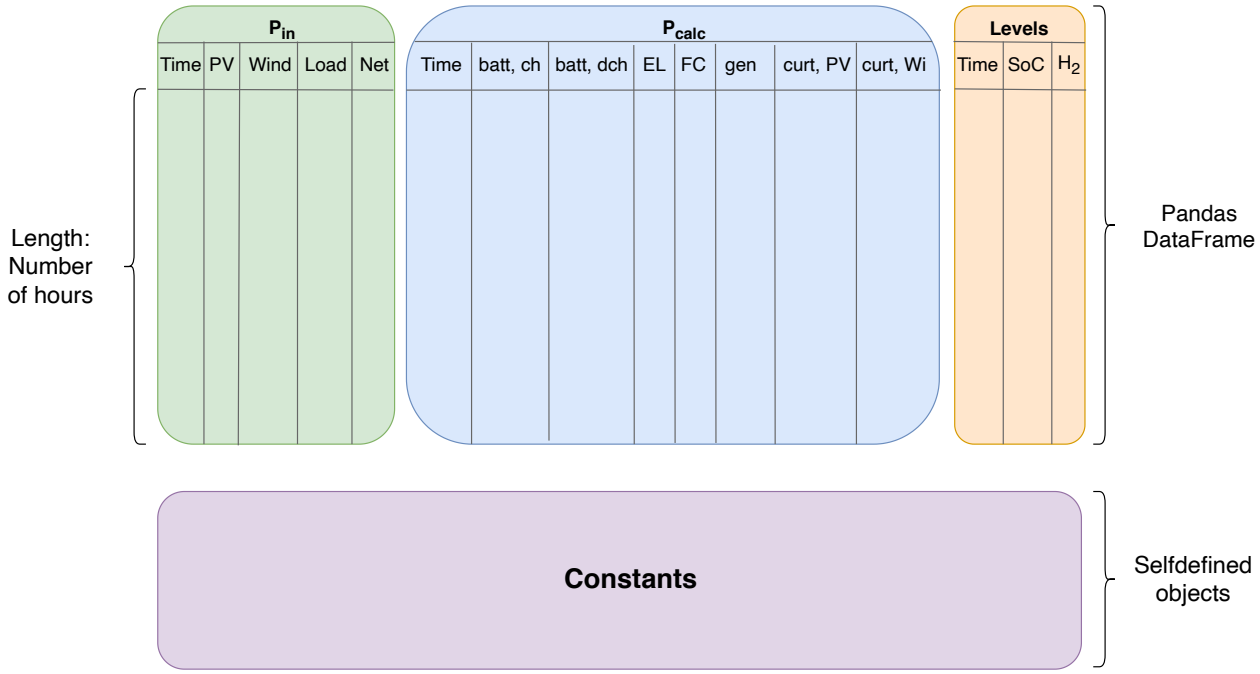

Figure 7.1: Data structures within the code for basecase control.

The Constants have attributes like ”type”, ”component”, ”command”, ”description” and ”limit”. Here ”limit” contains the value of the constant, while the other attributes together define the nature of the constant in question. Constants are for example used for battery SoC limits, power ratings and efficiencies.

The storage efficiency of the simulation could be improved by combining all these DataFrames in one. Doing so, the number of indexing columns (”Time”) would be reduced. The battery columns (charge and discharge) could also be combined. For a solution that is deployed in a live system in a remote area, storage considerations may be important. One should then further optimize the datastructures. However, as this is a one-time simulation with a limited amount of data points (8760) readability of the code was considered more important.

Data preparation details

As described in section 4.4, a lot of alterations had to be made to the original dataset in order to make it coherent. The details on which timings had to be altered in the wind and PV data are given in this section.

Alterations and missing values in the PV-dataset:

- **6/12-19 1:00 - 31/12-19 23:00, Power:** Generated by renewables.ninja, with the MERRA-2 dataset from 2019 with a capacity of 89 kW, a system loss of 5%, a tilt of 35°and an azimuth of 180°.
- **6/12-19 1:00 - 31/12-19 23:00, Temperature:** The temperatures given renewables.ninja has reasonable fluctuations, but was shifted to lower temperatures. By comparing the temperatures from renewables.ninja and SolarEdge, it was found that those from SolarEdge (which are measured on site) were in general 2.46°C higher. The temperatures in the period 6/12-19 1:00 - 31/12-19 23:00 are therefore those found by renewables.ninja, shifted upwards by 2.46°C.
- **6/12-19 1:00 - 31/12-19, Irradiance:** The irradiances given by renewables.ninja were very different from those measured on site. As this would have made the machine learning predictions inaccurate, another solution was found. The irradiance levels were reverse-engineered by looking at the power generation and inserting an irradiance level that previously yielded similar powers.
- **1/1-20 00:00 - 9/1-20 13:00, All:** As little PV-data was available from other sources for 2020 and this period was rather short, the first nine days of January 2020 were filled in with data from 10/1-20 00:00 - 19/1/20 13:00.
- **30/1-20 13:00 - 5/2-20 8:00, Power** For most of this period, the measured temperature and irradiance was available. A machine learning model was built on previous data (april-november), and predicted the output power of the panels.
- **4/2-20 16:00 - 5/2-20 8:00, All:** None of the parameters are available here. As all of the datapoints are during times when there is no sun and therefore no power generation it is of little importance. All the datapoints were therefore substituted with the values from the following day.
- **Minor holes:** A number of smaller holes were found, typically 1-7 hours missing at a time. These were 8/10-19 09:00-12:00, 22/2-20 12:00-18:00, 28/3-20 11:00 and 29/3-20 02:00. As these were limited in timespan it was decided that each parameter (power, temperature and irradiance) was replaced by a linear function between the previous and coming data points.

Alterations and missing values in the wind-dataset:

- **Linear replacement:**
  - 1/4-19 23:50 - 2/4-19 00:50
  - 11/4-19 10:30
  - 25/5-19 11:00
  - 23/10-19 10:10-10:20
  - 12/11-19 11:00-11:20
  - 11/12-19 2:20-3:30

  - 11/12-19 3:40-4:40
  - 11/12-19 10:40
  - 17/1-20 12:00-12:10
  - 20/1-20 16:20
  - 31/1-20 11:30-11:40

- **Replaced by previous:**
  - 8/10-19 9:00-12:50
  - 8/10-19 13:00 - 9/10-19 12:20
  - 10/12-19 19:10-22:00
  - 1/1-20 5:00-9:40
  - 4/1-20 3:00-8:20
  - 4/2-20 15:40 - 4/2-20 9:20
  - 22/2-20 12:20-19:00

NTNU
Norwegian University of
Science and Technology

TrønderEnergi®